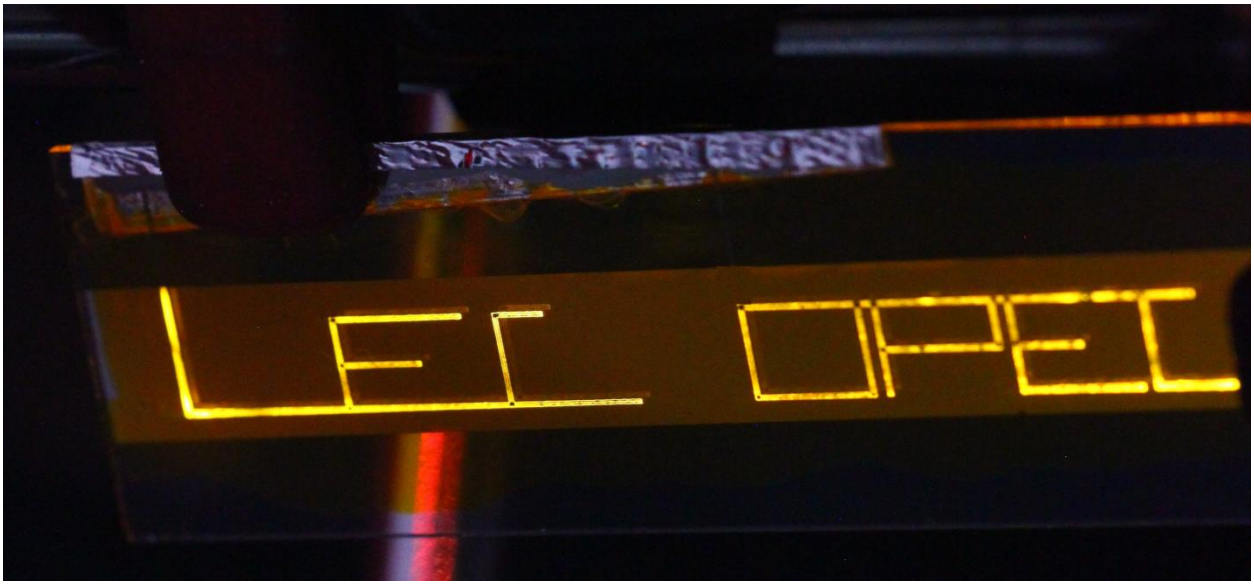

In Quest of Printed Electrodes for Light-emitting Electrochemical Cells: A Comparative Study between Two Silver Inks

Masrur Morshed Nahid

Supervisor: Andreas Sandström
Examiner: Ludvig Edman

Master Thesis in Physics 60 ECTS-credits
2012-12-10
The Organic Photonics and Electronics Group (OPEG), Department of Physics, Linnaeus Väg 20, Umeå University, SE-901 87 Umeå

Acknowledgements

For your suggestion, supervision, guidance, support and encouragement, thank you very much

Andreas Sandström

Ludvig Edman

My heartfelt gratitude goes to

Amir, Christian, Jenny, Jia, Nikolai, Roushdey, Shi

as well as to

Mamun, Shibbir, and my soul-mate, Rima

Abstract

This thesis presents a comparative study between two silver nanoparticle inks that were deposited using a Drop-on-Demand (DoD) inkjet printer, aiming at finding a functional ink that can be used to print electrodes in Light-emitting Electrochemical Cells (LECs). To achieve this, a DoD inkjet printer was installed and an acquaintance with the printer was attained. Among the two inks, one was employed as received while the other was reformulated, and successful deposition of both the inks was observed. During the reformulation process, it was seen that the highly volatile tetrahydrofuran (THF) solvent can be used to improve the ink properties, in contrast to what is recommended. After that, the inks were deposited on UV-ozone treated glass substrates, sintered at an elevated temperature under ambient conditions, and their specific resistances and thicknesses were measured. Finally, the inks were used to print the anode in a structured sandwich-cell LEC. The performance comparison was conducted by observing the emitted light of the LECs. The results indicate that the reformulated ink performs better, probably due to the lower silver concentration that results in flatter surface, which in turn effectively alleviates shorts.

Contents

1 Purpose of the Thesis

The Organic Photonics and Electronics Group (OPEG) at the department of physics of Umeå University has recently acquired a Drop-on-Demand (DoD) material deposition inkjet printer. It will allow new avenues forward regarding design, fabrication, and development of flexible electronic devices. One such device is the Light-emitting Electrochemical Cell (LEC), a complex entity that combines the sciences of organic chemistry and solid state physics, and which has been extensively researched in the OPEG labs.[1-7] Today, this research is primarily focused on solution processable light-emitting polymers and electrolyte systems, but a different aspect, by no means less crucial, is the required electrodes that connect the LEC to an external power-supply,[6, 8] and finding methods of applying these using solution based processes. Though tremendous effort has been aimed world-wide at finding highly conducting materials with high transparency, no obvious replacements for current vacuum deposited electrodes exist. The ink-jet method has the potential to solve some of these issues, especially when a DoD deposition technique is used, since it allows for a precise deposition of a variety of materials thus allowing clever electrode designs to be employed. The DMP-2800 DoD material deposition inkjet printer (FUJIFILM Dimatix Inc., USA) has been procured for this very reason: depositing nano-sized metallic particles with high accuracy allowing highly conductive and functional LEC electrodes.

The focus of this thesis is to compare two types of inks comprising nano-sized silver particles. This was done by installing and employing a DoD DMP-2800 inkjet printer to deposit the inks. The inks were evaluated by looking at the physical characteristics of printed Ag-traces. In addition, this thesis encompasses a comparative study of the performance of LEC devices in which the printed electrodes were employed as the anode. To achieve these objectives, an acquaintance with the DMP-2800 was attained followed by a necessary ink formulation study where one of the Ag-ink was mixed with various additives to make it compatible with the printer. The inks were deposited on UV-ozone treated microscopic glass substrates and sintered, after which the specific resistance and the thickness were measured. In addition to this, a change in appearance of one of the inks was reported while stored in air. After that, the inks were also used to make electrodes in LEC devices by sandwiching a drop-casted organic light-generating material between printed Ag-electrodes and an evaporated Al cathode.[9, 10] A constant external voltage bias was applied to light up the devices and to study their performances. In addition, this thesis contains practical guidelines on how to best utilize the printer and the inks, and possible future projects are proposed.

2 DMP-2800 Inkjet Printer: An Introduction

The DMP-2800 is a software controlled DoD inkjet printer that allows the user to deposit fluid materials on an A4-sized substrate (210 mm x315 mm) using a piezo-based inkjet cartridge. The complete system is shown in figure 1. This table-top printing device comprises a print-head, ink cartridges, a vacuum controlled substrate holder, two cameras, a stepper motor controlled x, y, and z stage, and a computer with pre-installed software. The individual parts of the printer and the software will be described in more detail below.

Figure 1: Dimatix Materials Printer, DMP-2800 (FUJIFILM Dimatix Inc., USA), and the PC that is used to control the printer.

2.1 Hardware Configuration of the machine

The print-head consists of disposable cartridges with a maximum reservoir-capacity of 1.5 ml of user-fillable fluid, as shown in figure 2a. Each cartridge has 16 Micro-Electro-Mechanical System (MEMS) based nozzles, placed in-line at a distance of 254 μm apart from each other. The diameter of each nozzle, the drop size generated through that nozzle, and the operating frequency of the jetted fluid depend on the cartridge type. The two types of cartridges that are compatible with the DMP-2800 are DMC-11601 and DMC-11610, which contain 9 μm and 21 μm diameter nozzles, and produce nominal drops of 1 pl and 10 pl (±20% adjustability), with a maximum operating frequency of 15 kHz and 60 kHz, respectively. The print-head also comprises of a built-in heater with a maximum heating capability of 70°C (±1°C variability).[11]

a **b**

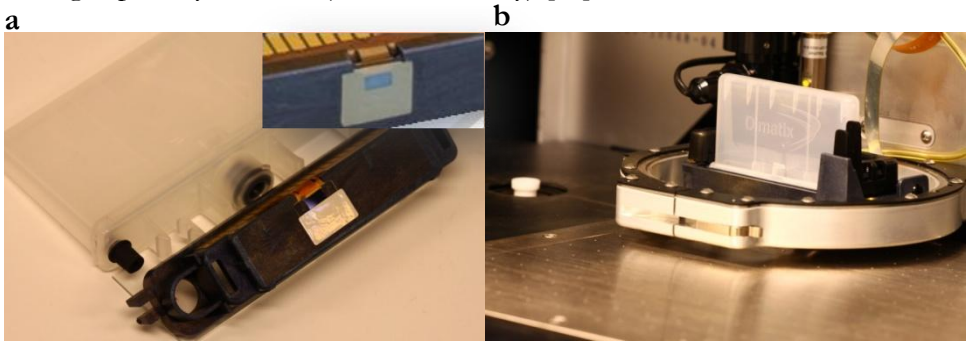

Figure 2: a) DMC-11610 Cartridge, with the white reservoir and the MEMS controlled nozzle module separated from each other. The nozzles are placed in the blue area shown in the inset. b) Print-carriage with the installed cartridge, on top of the perforated and heatable platen and the cleaning station (at the left).

The substrate-holder, seen in the lower part of figure 2b, is a perforated metal platen connected to a vacuum pump. It has a built-in heater able to heat the platen up to 60°C (±2°C uniformity), and can hold up to 25 mm thick substrates. The substrate is placed on top of the platen and the platen is scanned in the *x* and *y*-direction to achieve a raster-style printing.

The fiducial camera is mounted on the cartridge and it is used to align the substrate on the platen and to inspect the printed pattern. It can be used to measure the size of the printed drops directly, important when determining the print resolution. The software controlling the camera contains a feature for measuring the head angle (saber angle), which permits the user to verify whether the manually set head angle is correct. Also, it contains several features that help the user to fix the offset of the placed substrate, to align with the printing axes, to save photos in .bmp format or to set a print reference/print origin of the pattern. Particularly, these features help the user to keep track of the pattern when a new substrate replaces an old one, when a cartridge with a new fluid is introduced, or when a new print operation is launched.

The drop-watcher camera is a stroboscopic, built-in deposition observation system that allows the user to inspect the drop formation at the nozzle/air interface. The camera image on the monitor screen is a 150-fold magnification of about 210 mm x 170 mm, so that it represents an actual area of about 1.4 mm x 1.1 mm.[11] The user can watch the drops in fixed static positions (image-like) as well as under motion (video-like) when they are ejected from the nozzles. Using the drop watcher, the drop velocity can be measured manually using the velocity markings displayed on the monitor. Photos and videos of the process can be saved in the .bmp and .avi format, respectively.

The cleaning station comprises disposable cleaning pads that are used to clean the nozzles of the cartridge (see figure 2b). Three methods of cleaning can be performed: purge, blot and spit. Purge is used to ensure that all the channels in the cartridge are filled and free from air bubbles, blot is used to remove any drops formed beside the nozzles, and spit is used to remove any clogging formed at the nozzle orifice. These software-driven cleaning methods can be run individually or can be combined as a cleaning cycle. Typically, a cleaning cycle consists of purging and blotting for a few seconds. If the fluid used is prone to clogging, spitting is also added to the cycle.

2.2 Dimatix Drop Manager Software

The Dimatix Drop Manager is the PC-based Graphical User Interface (GUI) application software of the DMP-2800 inkjet printer that allows the user to control it by means of a USB- and a video-in cable. The main screen of this PC-user interface software (see figure 3) consists of three pull-down menus: 'File', 'Tools', and 'Help'; four segments: 'Install Cartridge', 'Select Pattern', 'Load/Unload Substrate', and 'Print Set-up'; three tabs: 'Drop Watcher', 'Fiducial Camera', and 'Run Cleaning Cycle'; and two navigating tabs: 'Back' and 'Next'.

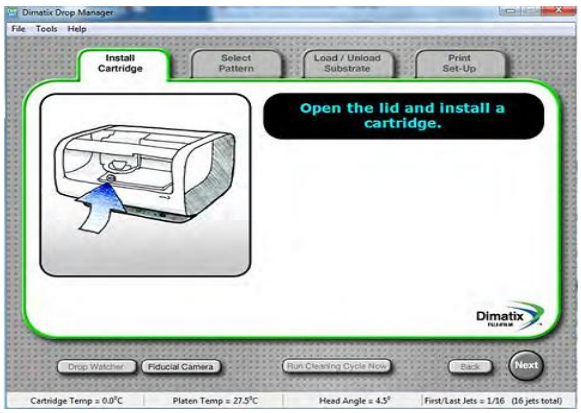

Figure 3: Main screen of the Dimatix Drop Manager software.

Whenever a new ink cartridge is installed, the cartridge settings window (see figure 4) is used to input and establish the correct parameters with the help of the drop-watcher camera. The window contains three tabs: 'Waveform', 'Cartridge', and 'Cleaning Cycles'. The 'Waveform' tab (see figure 4a) contains the 'Jetting Voltage' buttons for all the 16 nozzles. These buttons allow the user to regulate the voltage of each nozzle individually (in the range of 0 to 40 V). This individual voltage regulation is particularly important because the velocity of the drop formed at a nozzle is a function of voltage applied to that particular nozzle. This tab also contains a 'Tickle Control' on/off button (with frequency adjustability) that enables and controls the low amplitude pulse that is given to the nozzles periodically to move the meniscus slightly but not to eject a drop. The 'Cartridge' tab (see figure 4b) contains four buttons: 'Cartridge Temperature (°C)' for controlling the jetting temperature (in the range of ambient to 70°C), 'Meniscus Vacuum' for controlling the meniscus pressure (in the range of 0 to 6 inches of water), 'Jets to Use' for selecting the adjacent jetting nozzles, and 'Cartridge Print Height' for setting the distance of the print-head above the substrate (in the range of 0.25 mm to 1.5 mm). The 'Cleaning Cycles' tab (see figure 4c) contains four buttons that allow the user to maintain and create cleaning cycles before, during, and after the printing action as well as when the printer is idle.

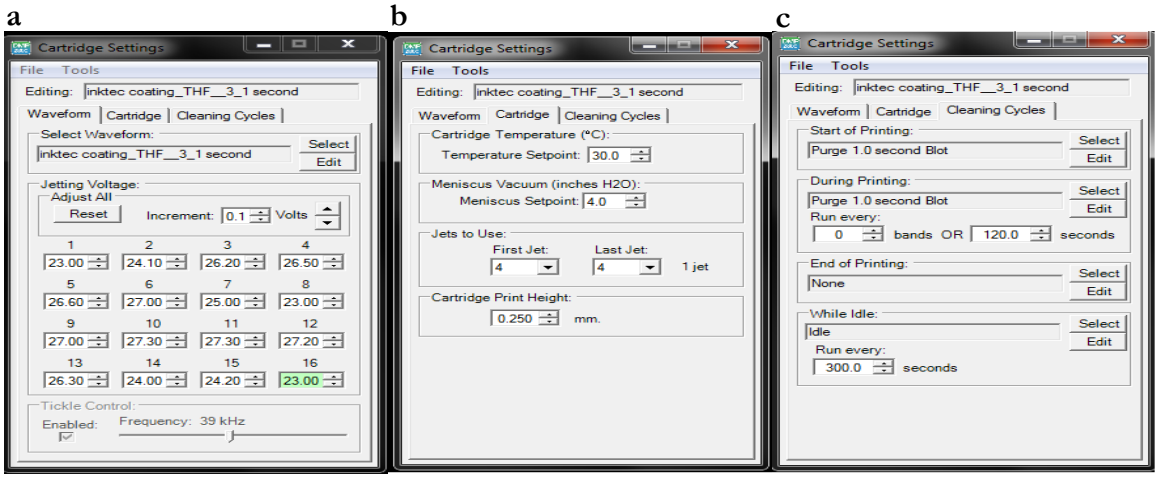

Figure 4: Cartridge settings window showing a) Waveform tab, b) Cartridge tab, and c) Cleaning Cycles tab.

The edit button in the 'Waveform' tab of the cartridge settings window opens the waveform editor window, as can be seen in figure 14. This window consists of two graphs: 'Jetting waveform' and 'Non-Jetting Waveform', which allows the user to adjust the whole jetting process (the drop formation, velocity, drop-size etc.) with the help of the drop-watcher camera. Clicking a segment in the jetting or non-jetting waveform enables the user to adjust the required parameters in that segment.

The 'Pattern Editor' option can be accessed through the 'Tools' pull-down menu of the main screen window. This enables the user to make patterns with a desired resolution by setting the drop spacing (in μm) that is consistent with the head angle, substrate-fluid pair, and the drop size. The buttons in the window allow the user to draw patterns by portraying/canceling rectangular segments with the help of a preview window. Also, in this section, the user can fix the reference point/print origin, print a repetitive array of the designed pattern, and set the number of layers that the printer should reprint automatically over the same pattern. The Dimatix Drop Manager software can import the .bmp images and can process those images into pattern files through the 'Pattern Editor (Bitmap Images)' window. This window also comprises different sections and buttons that allow the user to watch and work with the imported image systematically.

The print set-up segment in the main screen window allows the user a final affirmation of all the required parameters before a printing job starts and to confirm/cancel the printing. This window summarizes all the required fields and allows the user to set the substrate thickness, jetting temperature, the platen temperature, and to toggle the substrate holder vacuum pump on/off.

3 DMP-2800 Inkjet Printer: An Overview

The DMP-2800 is a DoD printer that is designed in the *bend*-mode configuration, as shown in figure 6, where the print-head is equipped with a piezoelectric transducer, which allows the user, depending on the cartridge used, to create and eject 10 pl or 1 pl nominal drops by applying a time varying voltage signal that is converted into translational motion by the receiving transducer. In practice, the liquids employed must have properties that fulfill those of the so called 'functional fluid'. The ink, and the substrate used, brings performance limits such as a minimum size of individual drops and a minimum line width when making a continuous trace. However, even with an ideal ink, the DMP-2800 has mechanical limits that restrict the deposition to a maximum of 5080 drops per inch with a minimum drop size of 5 μm at a head-angle of 1.1°.

3.1 Advancement of the Printing Technology

The first crude inkjet device was patented by William Thompson in 1858.[13] Since then, inkjet printing has matured and developed into a versatile and promising drop deposition technique. However, even though the concept has improved over the 150 years it has existed, the principal function still remains the same: the formation and deposition of droplets with the desired volume and jetting velocity from both Newtonian and non-Newtonian fluids. Various methods have been employed to achieve this, but most are found within two major categories: the Continuous Ink Jet (CIJ) technology and the DoD technology. Though both technologies emerged commercially in the 1960s[14], scientists and commercial printer-manufacturers still find interest in both of them. In spite of the fact that both technologies have developed over time, none can be said to completely eclipse the other as each still got its own advantages. In CIJs, streams of ink droplets are formed by the Rayleigh instability. These droplets are ejected under pressure through a nozzle with a typical velocity of 10 ms^{-1} and a frequency of 20-60 kHz. A schematic of the drop ejection mechanism of CIJ technology is shown in figure 5a. The nozzle is subjected to a voltage bias that imparts a charge on each drop as it is formed. After ejection, each drop is subjected to a further voltage bias that imparts a deflection of the drop to an angle proportional to the induced charge. Since by definition, CIJ printer jets the ink continuously, a majority of the drops is not deflected for printing and only a fraction of the ejected drops is actually used. The non-printed drops are collected in a gutter where a pump is used to re-circulate the drops to the ink chamber. Though, this technology permits relatively long distances between the nozzle and the substrate, no nozzle-clogging, and offers the fastest inkjet printing, it still suffers from several drawbacks, such as the need for high-pressure maintenance to supply the ink to the nozzle orifice, the complicated hardware needed to synchronize the breakup of the drops when more than one nozzle is used, using only a fraction of the ink to print, continuous re-circulation of the non-printed drops to limit the amount of waste etc.[13, 15] On the other hand, in DoD technology, ink droplets are formed by propagating a pressure pulse in the fluid held in a chamber. A schematic of this mechanism is shown in figure 5b. In this case, when the pressure is more than a threshold limit, a drop is ejected. In the absence of the pressure, the ink is held in the chamber because of the surface tension of the fluid. Also, a static pressure is maintained to make sure that the meniscus at the orifice is stable. Hence, by definition, the drops are ejected on-demand, as can be seen from the schematic. In this case, the drop

deposition is achieved by positioning the substrate under the nozzle before ejection of a drop. Though DoD printers are operated at a lower frequency, typically 1-20 kHz, they offer a practically uncomplicated, economically favored, and fairly straightforward method that makes the process a lot easier and hence more favorable, especially when small amounts of expensive inks are employed.[16, 17]

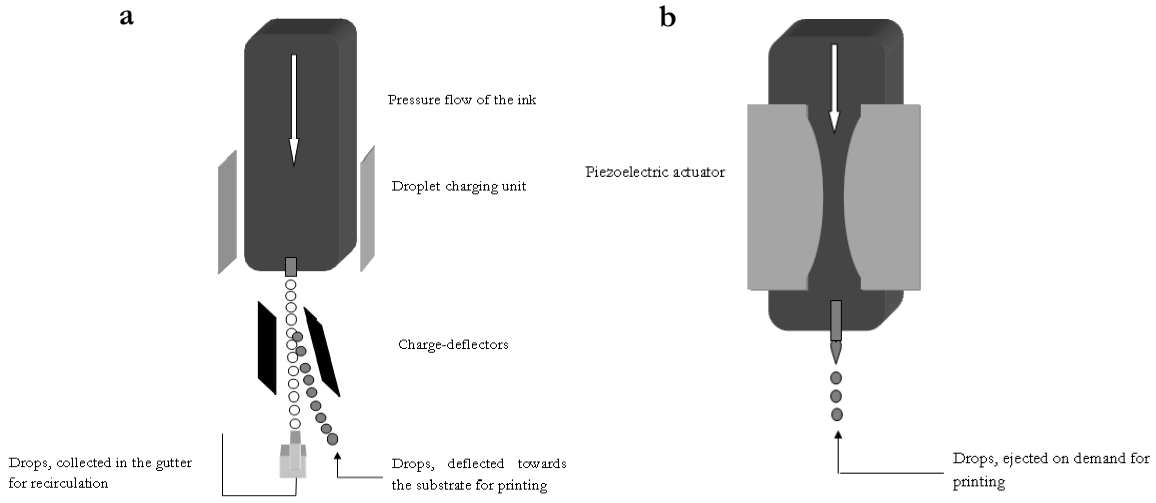

Figure 5: Schematics showing drop ejection mechanism of a) CIJ technology and b) DoD technology (piezo-actuator based).

In order to generate pressure to the actuator, several schemes are used in DoD based printers. Among them, the two most common schemes are thermal and piezo based printers. In thermal inkjet printers, the pressure is generated by vapor bubbles which are created by the local heating of the ink. This limits the diversity of the ink as well as the durability of the print-head. In comparison, piezo-actuator based inkjet printers can print almost all liquids while the printed drop volume ranges from nanoliters to a few picoliters. Another advantage of the piezo inkjet printers over the thermal printers is that the piezo materials can be used in different deformation modes, which allows for large design flexibility. The most realistic designs are *squeeze*-mode, *bend*-mode, *push*-mode, and *shear*-mode.[14] Figure 5b and 6 exemplify the *squeeze*-mode and the *bend*-mode design configurations, respectively.[18]

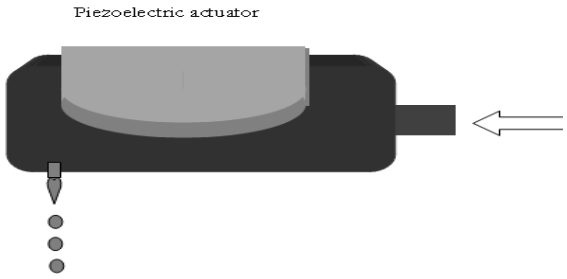

Figure 6: Schematic showing drop ejection mechanism in bend-mode design configuration.

3.2 The PZT-MEMS Device Theory

This piezo-based DoD inkjet is based on the coupling between the electrical regime and the mechanical domain through the piezo-electric actuator, and the coupling between the acoustic regime and the fluid-dynamics domain through the drop formation mechanism. The electro-mechanical coupling is achieved using MEMS technology, while the acoustic-fluid dynamics coupling is achieved by tuning the input voltage waveform that deforms the fluid chamber. The combination of these two mechanisms facilitates the print-head of the DMP-2800.

In the *bend*-mode design, the piezo material is etched with each of the channels (fluid chambers) in such a way that the externally applied electric field aligns in the direction parallel to the polarization of the piezo material. The piezo material which is used here is lead-zirconate-titanate ceramics, $Pb(Zr_{0.53}Ti_{0.47})O_3$ (PZT). Each channel of the print-head is actuated by the PZT, i.e. the systematic deformation of the PZT causes the suction of the ink into the chamber (from the reservoir) as well as the jetting of the ink through the nozzle (as a single droplet). The schematics shown in figure 7 visualize this process. This channel-PZT combination needs to deform as a single unit and this deformation needs to be synchronized to the applied electric field. In order to accomplish this, each channel-PZT unit of the DMP-2800 print-head is constructed using single crystalline silicon. Since the thermal expansion coefficient of silicon is close to that of PZT, the combination of the two materials ensures that the entire unit expands relatively uniformly and without stress under any thermal load. Also, other inherent properties like the chemical resistivity, the single-crystal structure, the lightness, as well as the stiffness make silicon an excellent choice as an integral part in the print-head.

3.3 Functional-Fluid Characteristics

The functional fluid (the ink) is a material that must be compatible with the printer, and certain criteria need to be fulfilled for a fluid to be functional. This is due to the physics of the drop formation, i.e. jetting the drops out of the nozzle, which essentially is very complex as it depends on the forces involved in the fluid-statics and the fluid-dynamics as well as on the geometry and the material properties of the fluid chamber. The schematic of figure 7 illustrates what happens when the forward and reverse pressure in invoked in the chamber. The fluidic forces, e.g. viscosity, surface tension, inertial force, compressibility etc., dominate the fluid-flow upon invoking the forward pressure in the chamber. Also, the pressure becomes attenuated and reflected because of the geometry and the material of the chamber. Thus, a spatial propagation of the fluid as a function of time is realized. Near the nozzle, other factors, such as fluid-air interaction, surface tension, temperature, capillary forces etc., make the propagation function even more complicated. As a result, drops are formed as illustrated by the schematic in figure 7a. Again, just after forming the drop, the nascent fluid is needed to pull back at the right time to break-off the drop and thus, a backward pressure is also needed. Figure 7b illustrates the result when a sufficient backward pressure is invoked. Hence, in order to form the drop of the functional fluid, this pressure must be sufficient enough so that it can force the fluid to overcome the fluidic forces, impart momentum to the fluid to jet the drop with a required velocity, and can work in the opposite direction to pull-back the nascent fluid at the right moment to break-off a droplet.

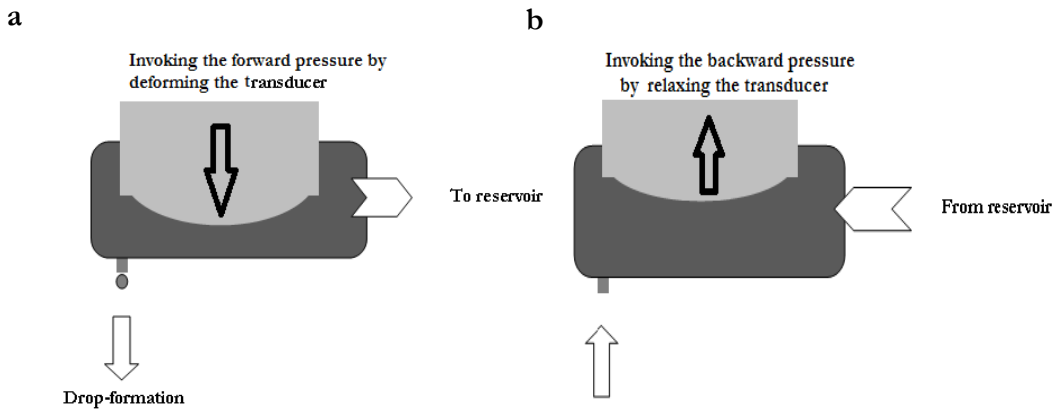

Figure 7: Schematics illustrating working principle of drop-formation: a) when the forward pressure is invoked, and b) when the backward pressure is invoked. Note that the fluid flows in the opposite directions, depending on the directions of the invoked pressure, as indicated by the arrows.

In case of the DMP-2800, the actuator can generate the required back-and-forth pressure for fluids with certain properties. In order to be compatible with the mechanical-electrical system of the printer as well as with the dimensions of the print-head (i.e. nozzle, nozzle spacing), the functional fluids must have properties that fall within a defined window. The fluid can be aqueous or solvent-based, and both solutions and particle suspensions can work. For good performance, the fluids should have a viscosity of 10-12 cps (0.01-0.012 pascal-sec) at the jetting temperature, though it is possible to jet the fluid with a viscosity as high as 30 cps (0.03 pascal-sec). Also, for the desired performance, the functional fluid should have a surface tension between 28-42 dynes/cm (0.028-0.042 N/m) at the jetting temperature, though fluids having a surface tension as high as 60 dynes/cm (0.06 N/m) can be jetted. Additionally, to prevent the fluid-drop from drying at the nozzle/air interface, fluids having a low evaporation-rate and a boiling point higher than 100°C are preferable.[12] The fluid is preferably filtered before use to remove large agglomerates, fibrous particles, or gels. Also, a pH-value between 4 and 9 is recommended. For some fluids, especially aqueous-based, degassing might be necessary to remove any dissolved gas which could inhibit jetting.

The DMP-2800 inkjet printer is developed to jet functional fluids that have the aforementioned properties, but fluids outside this range can also be jetted, albeit with lower jetting performance. In some cases, the fluids need to be reformulated to achieve properties closer to those of the functional fluid. This is necessary when the viscosity, surface tension and/or evaporation-rate of the original fluid do not fall within the defined window of the functional fluid. This is normally achieved by trial and error, employing additives in different ratios to change the properties of the fluid, and testing the performance using the drop watcher. Additives involve (but are not limited to): surfactants, such as carboxylates; solvents, such as tetrahydrofuran; and/or humectants, such as glycol. Simultaneous manipulation of the jetting waveforms, the temperature, and the meniscus pressure while characterizing the velocity and the drop-formation, are important during the trials. Other influencing factors that need careful consideration are the cleaning cycle, non-jetting waveform, fluid-substrate pair, letting the ink settle in the cartridge for a specific time before installing it in the machine, and

keeping the nozzle-areas of the cartridge clean etc. Though the reformulation of the ink may result in lower performances in the firing frequency, drop velocity, drop formation and sustainability, it should create spherical drops of sufficient volume without any tailing effect. As an example, figure 8 displays drops that were formed with a reformulated ink at only 2 kHz firing frequency, but which exhibits spherical drops jetted at a ~7 ms^{-1} velocity without any tailing effect.

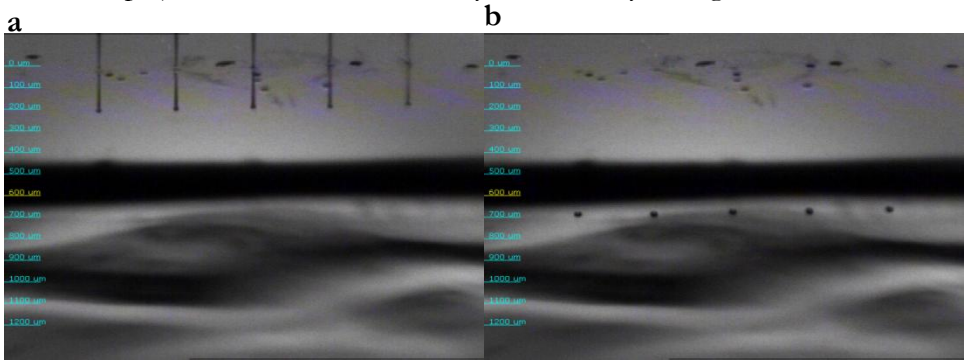

Figure 8: Stroboscopic drop formation photos captured by the drop watcher camera showing a) the tailing effect at ~30 μs, just after the drops come out from the nozzles and b) fine spherical drops without any tailing effect at ~100 μs ejected at a velocity of ~7 ms^{-1}.

3.4 Waveform Basics

The waveform gives the user control over the printing mechanism. The user can change the parameters, e.g. jetting frequency, voltage, amplitude level, slew-rate, and pulse-duration, which results in a change of the acoustic pressure acting on the fluid. This in turn changes the process of formation and break-off of the droplets out of the nozzle. The user needs to develop the waveform in parallel with the fluid. The typical basic waveform, or firing cycle, is divided into three/four segments as shown in figure 9, where each segment has three adjustable properties: slew-rate, level, and duration. However, as shown in figure 9a, the waveform also comprises a segment 0, but it is actually connected to segment 4; naming it differently is done only for the sake of understanding the waveform mechanism in a systematic and efficient manner. The level (in percentage) is the amplitude of the applied voltage to the operating nozzle that determines how far the transducer is bending, the slew rate (in a scale of 0 to 2) is the slope of the applied voltage that determines how fast the transducer is bending, and the duration (in μs) is the time of the applied voltage that determines how long the transducer will stay in that position. During segments 1 and 2, the drop is formed and jetted, while the last two segments define the drop break-off and the resetting of the unit for the next cycle.

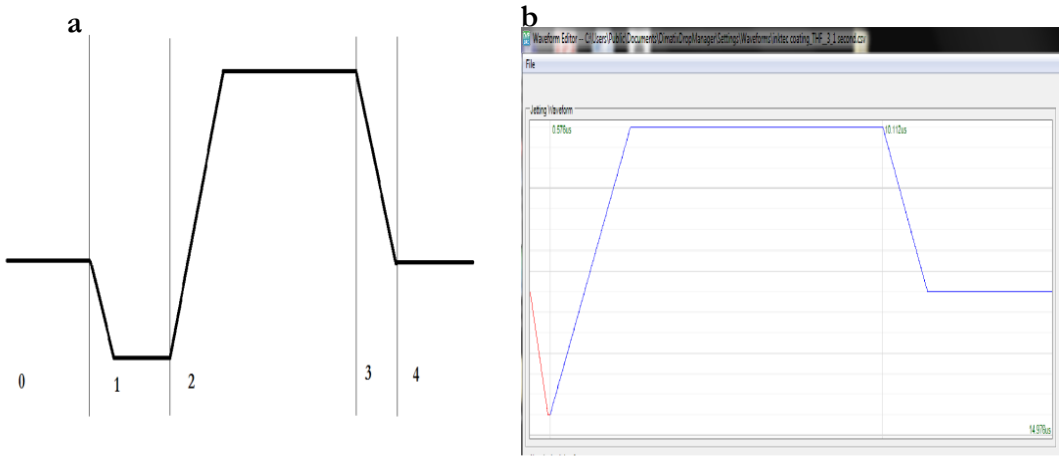

Figure 9: a) Schematic of a jetting waveform with different segments (not in scale) and b) screenshot showing an example of the jetting waveform as it can be seen in the waveform editor window.

As illustrated in figure 9a, a voltage is applied at the beginning, i.e. segment 0 and 4, so that the transducer is warped slightly. The starting of the firing cycle is represented by segment 1. At first, when the firing starts, the transducer is reset back to its neutral state (relaxing state) by applying 0 V (0% level), as can be seen at segment 1 and the red segment of figure 9b. At this state, the fluid chamber achieves its maximum volume and fluid is pulled in through the inlet, while the meniscus is pulled inward at the nozzle orifice, as demonstrated earlier by figure 7b. The next phase, segment 2, is the main drop ejection phase where the transducer is pushed to its maximum state by applying 100% of the applied voltage, as shown in the schematics as well in the screenshot. At this state, the fluid chamber reaches its minimum volume and the fluid is pushed out of the nozzle orifice, helped additionally by acoustic effects (see figure 7a for further demonstration). The slew-rate and the time duration define the timing of the firing of the fluid. Just after the firing pulse, the recovery phase is applied in segment 3 and 4 where the transducer is pulled back to a partially relaxing position. At this state, the fluid chamber gets a partial volume, the chamber is decompressed and the fluid is partially refilled for the next cycle.

In order to get a higher firing velocity, the slew-rate is recommended to be lower in segment 1 and 2 and higher in segment 3 and 4. Initially, a higher voltage is also recommended which can be subsequently lowered when a satisfactory drop formation is observed. Additionally, since the first two segments have the most impact on the velocity and the drop formation, the parameters of these segments are needed to be dealt carefully while the parameters of the last two segments are merely needed for the fine tuning of the drop formation.

Also, depending on the fluid used, a non-jetting waveform is needed. This waveform works in the same way as described above but it is executed continuously to keep the nozzle ready for the firing cycle. For non-jetting waveforms, the voltage amplitude is set at a lower level so that the ink in the chamber is subjected to a dynamic pressure, without causing a drop to be ejected. It is also explained in a later section and is shown in figure 15.

3.5 Printed Features: Resolution Parameters, Drop-Size and Limiting Factors

The printed features of the DMP-2800 printer depend on various factors: fluid and substrate characteristics, fluid-substrate interaction (adhesiveness), sintering conditions of the fluid, print-head temperature as well as substrate temperature, changing-viscosity of the fluid, drop-volume, head angle (saber angle), and drop-size on the substrate. Factors related to the fluid and substrate characteristics are porosity, surface energy and surface-smoothness of the substrate, the adhesiveness between the fluid-substrate pair, surface tension, viscosity, and compressibility of the fluid etc. These factors determine the properties like fluid-flow over the substrate surface, strength of the adhesive bond, wet-film formation etc. Since these parameters only depend on the fluid and the substrate, they need to be resolved before the printing operation. Also, factors related to the sintering conditions are temperature, method etc. These parameters determine the properties of the sintered material. Since these factors are inherent to the fluid used, they also need to be resolved before the printing operation. In addition, changing-viscosity of the fluid, jetting temperature and platen temperature can also affect the printing features. This is due to the fact that the fluid may be blended with surfactants, solvents, and/or humectants, which might require tuning of temperature as well as meniscus pressure. Since these issues are to be faced while tuning the drop formation, they need to be resolved before characterizing the printed feature.

For a particular fluid-substrate pair and jetting parameters, the resolution of the printed pattern depends directly on the drop-size and the head-angle (saber angle). As the schematics in figure 10 illustrate, the printer carriage and the platen move in such a way that the printing operation is done in a raster-style manner; the carriage moves horizontally (x-direction) while the platen moves vertically (y-direction). Since the printing nozzles are situated in a single line, the jetting nozzles move over the platen following a single line in the x-direction, as shown in see figure 10a. As the drops form in a single line following a raster-style printing, the user-set head-angle fixes the line to move at a certain angle with respect to the x-direction, as can be seen from figure 10c, which lowers the effective spacing between the nozzles. This results in the partial overlap of the drops that ultimately defines the print resolution. For a certain fluid-substrate pair, the user needs to determine the drop-size and in order to find out the drop-size, a recommended printing pattern, called 'test-pattern', is printed while the head-angle is kept at 90°, i.e. perpendicular to the direction of the cartridge movement, as illustrated by figure 10b. This results in a series of drops on the substrate. The user needs to inspect these drops with the fiducial camera and to measure the radius of the drops with the on-screen distance measuring feature. According to a chart given by FUJIFILM Dimatix Inc.[11], this radius value corresponds to a specific saber angle that in turn corresponds with the resolution of the printed pattern (in drop per inch values). This procedure is further exemplified in figure 16.

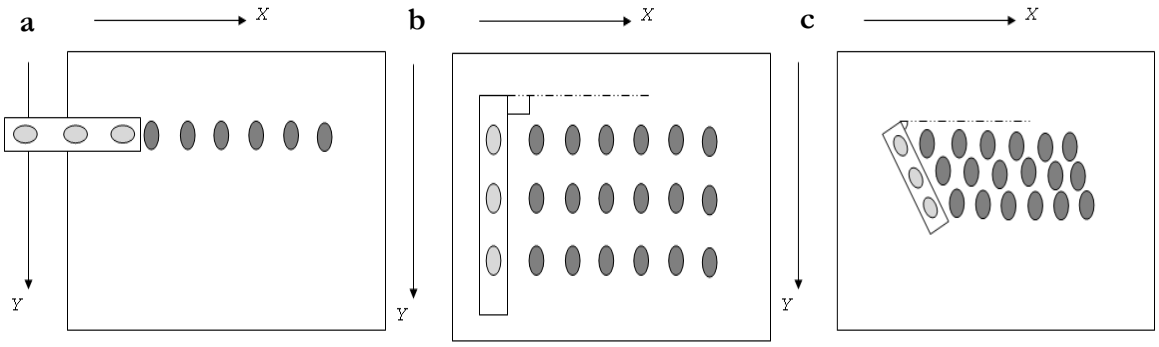

Figure 10: Schematics showing the raster style printing that explains the print resolution when the head-angle is kept at different angles with horizontal direction: a) at 0°, b) at 90° and c) at an angle in between. Note that only three nozzles and a single cartridge-sweep are shown in this illustration.

After measuring the drop-size, the user needs to insert the value in the pattern editor window and to set the corresponding head angle manually for investigation. The user needs to align the angle accurately, since an error here will distort the printed pattern. Hence, an experiment should be performed upon every change in head angle, where a printed trace in the *y* direction is inspected (see figure 11b). If the line consists of tilted line segments, the head angle needs to be adjusted. Additionally, a trace in the *x* direction is recommended, to ensure that the drops are ejected at a sufficient rate to achieve the sufficient spatial resolution (see figure 11a). As an example, when the experiment was performed in search for the possible finest resolution of the printed pattern that could be achieved with one of the Ag-inks on the glass substrate, line breaking and waviness were observed. In this example, horizontal and vertical lines of different widths were printed while the head-angles and drop-sizes were varied. The features can be seen from these experiments, where the head angle was fixed at 5.6° and the drop-size was fixed at 25 μm.

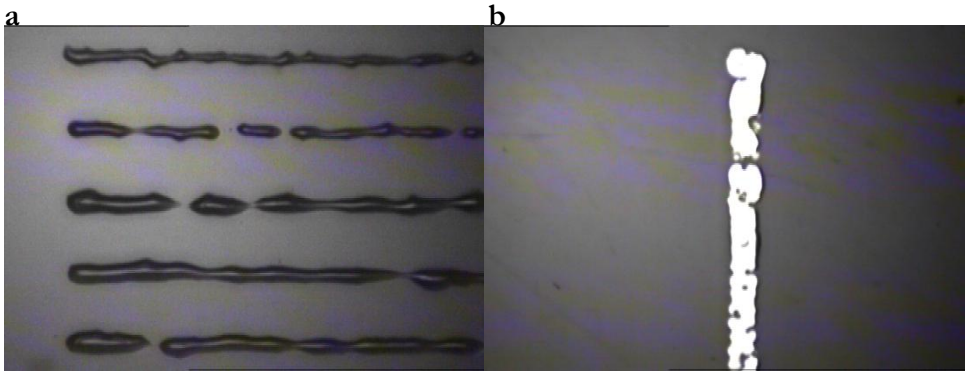

Figure 11: Lines printed with an Ag-ink illustrating the different features encountered while fixing the resolution of the pattern with the head angle fixed at 5.6° and the drop-size fixed at 25 μm; showing a) horizontal lines of 5 μm to 25 μm width and b) a vertical line of 40 μm width. Note that the photos were captured by the fiducial camera before sintering, just after the printing operation; that the widths were defined at the pattern editor window before printing; and importantly, that the head-angle was set manually.

The printed pattern, a single line for example, is determined by the user-defined deposition parameters. Since a series of drops make a line on the substrate, the parameters in this case are the same as mentioned above. In addition to those, there are other factors that restrain the printed pattern. Since the drops overlap differently depending on the drop-size and the head-angle, the width of the line in general can be affected; more commonly it causes 'scalloping' or 'waviness' at the edge of the line (see figure 12a). Also, the fluid may bead up and the line may break into individual spots (see figure 12b). When attempting to print thin lines, the user faces the fact that the waviness at the edges causes the line to break as the line-width reaches its minimum limit. Figure 12a shows beading of drops just after the printing operation and figure 12b shows the waviness because of this beading effect that in turn breaks the line. For this reason, the optimization between the surface tension of the fluid, surface properties of the substrate and the beading effect of the fluid is necessary. Hence, depending on the fluid-substrate pair and the sintering condition, the user needs to fix the drop-size first and then use a trial-and-error approach to establish the minimum line-width.

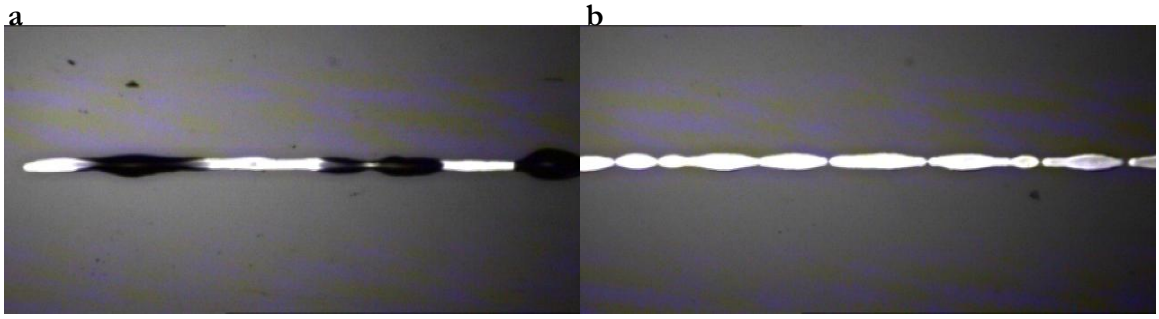

Figure 12: Single line of Ag nano particles (printed with Ink#1) deposited on the glass substrate (photos were captured by the fiducial camera) illustrating the waviness and the beading effects a) just after the printing operation and b) a few seconds later. Note that the photos were taken before sintering.

4 Ag-inks: Optimizing, Jetting and Sintering

This thesis-work comprises a systematic study of two different types of Ag-inks in order to compare their physical characteristics and their performances as the bottom electrodes of structured sandwich-cell LECs. These inks are: DGP-40TE-20C (ANP Co. Ltd., S. Korea)[19] and TEC-CO-011 (InkTec Co. Ltd., S. Korea).[20] Hereafter, the former will be referred to as Ink#1 and the latter as Ink#2. Pictures of the inks are shown in figure 13.

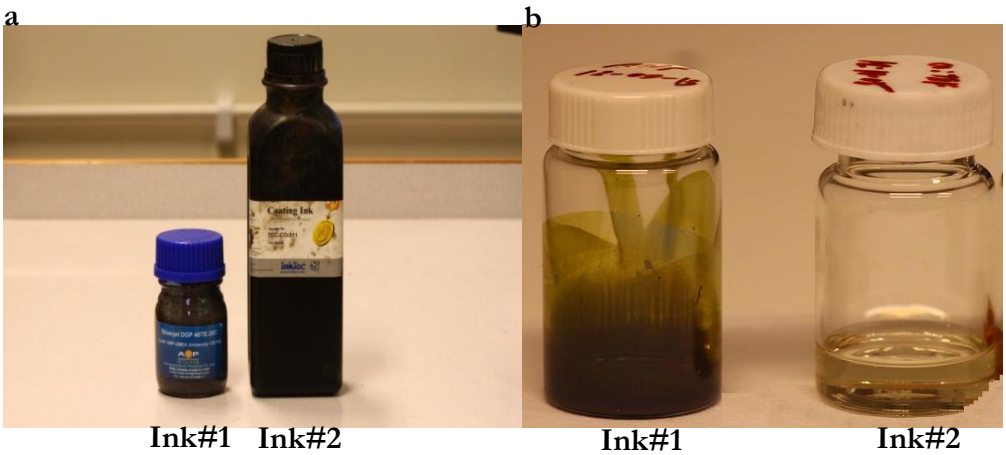

Figure 13: Ink#1 and Ink#2 as seen a) in the manufactures' supplied bottles and b) in the glass vials (~2ml). Note that Ink#1 was supplied in the glass container and Ink#2 was supplied in the black plastic container. Also note that the black 'absorbent' appearance of Ink#1 and the 'transparent water-like' appearance of Ink#2.

4.1 Difference between the inks

The differences between these inks should be noted. Ink#1 comprises ligand-capped metallic Ag-particles in a polar solvent (triethylene glycol monoethyl ether, TGME), which provide a high binding strength to the metal core and results in a stable ink. This ink is manufactured specifically for deposition on glass substrates using inkjet printers, such as the DMP-2800. On the other hand, Ink#2 comprises Ag nanoparticles in an organic matrix that contains solvents, polymeric compounds and dispersants. This ink is designed for plastic substrates, and optimized for spray or dip-coating. Table 1 presents the details of the inks.

Issues	Ink#1	Ink#2
Manufacturer	ANP Co. Ltd., S. Korea	InkTec Co. Ltd., S. Korea
Product No.	DGP-40TE-20C	TEC-CO-011
Manufactured for	Jetting	Coating (dipping/spray)
Recommended Substrates	ITO glass, Bare glass	Plastic
Price (per gram)	6.6 US $ (approx.)	0.4 US $ (approx.)
Dispersion Matrix	Polar solvent- triethylene glycol monoethyl ether (TGME)	Organic Compound-Unknown
Ag content (wt %)	31.09	10
Particle-size (nm)	≤50	≤40
Surface tension (dynes/cm)	36.6	25-29
Viscosity (cps)	16.2	7-13
Supplied in (see figure 13a)	Glass-container	Plastic Bottle (Black)
Appearance (see figure 13b)	Black, ink-like	Transparent, water-like
Storage condition	5-10˚C	0-5˚C
Sintering condition	~180˚C, 30-45 min on glass, in air	~120˚C, 3-15 min on plastic, in air

Table 1: Details of the inks.[19, 20]

4.2 Optimizing an Ink into a Functional Fluid

Since Ink#1 demonstrates all the required properties in order to be used as the functional fluid, it was employed as received. However, Ink#2 required a reformulation to jet with the DMP-2800 since the properties e.g. viscosity did not fall in the designated window. Though this ink is made particularly for spray- and dip-coating on plastics, it was observed that the adhesion with glass substrates was high enough to result in satisfactory conductive films following sintering. Being inspired from this fact, Ink#2 was reformulated and optimized into a functional fluid for jetting purposes. In doing so, a trial-and-error study was performed where several different solvents were added to the original ink in order to make it a functional fluid. In this study, the core focus was the tuning of viscosity and surface tension.

The best jetting performance was observed when tetrahydrofuran (THF) was mixed with Ink#2 in a ratio of Ink#2 : THF=3 : 1 (vol/vol) and subsequently jetted at 30°C cartridge temperature and at 4.0 inch water meniscus pressure. Having 0.48 cps viscosity and 28 dynes/cm surface tension, and appearing as a colorless-liquid, THF gave the best results by lowering the viscosity and the surface tension of the original ink. Though the surface tension of Ink#2 falls within the designated window, the viscosity does not. In addition, THF has a boiling point of 66°C that gives an advantage in printing with this Ink#2-THF mixture if the platen temperature is kept at ~60°C. This is because of the fact that the platen temperature causes almost instantaneous evaporation of the THF after the drop being placed on the glass substrate, leaving only the traces of Ink#2 which consequently turns into Ag-traces after sintering. It is important to note that even though the recommendation for the

functional fluid is that a boiling point of more than 100°C should be used, this study demonstrated otherwise. It is evidenced that adding solvents with lower boiling point and high evaporation rate can be advantageous, provided that the substrate temperature is kept near to the solvent's boiling point. The solvent may facilitate the optimization of the fluid and the jetting performance, but if it evaporates quickly on the substrate, then the deposited ink can be unaffected during sintering. This is particularly true when thin lines are printed, since a faster drying time alleviates the beading effect and line breaking

4.3 Adjusting the Jetting Parameters

The 10 pl DMC-11610 cartridges were exclusively used for the jetting of both the inks. Though 1 pl cartridges allow jetting with higher velocities than 10 pl cartridges, the 1 pl cartridges were not included in this particular thesis work, and the focus was instead placed on the comparative study of the ink properties and their performances as electrodes in a LEC configuration. Hence, jetting inks using 1 pl cartridges, and printing complicated and challenging print patterns, are left for future research.

Both inks were filtered through a 0.45 µm Teflon filter and kept in glass-vials under ambient conditions, as shown in figure 13b. The ink-filled cartridges were kept for more than 1 hour and a few initial cleaning cycles were carried out before jetting. In case of both the inks, the respective waveforms were optimized for spherical drop formation with minimized tailing effects at a jetting velocity of 5-7 ms^{-1}. The drop watching facility was used to watch the drops as they formed, while the jetting and non-jetting waveforms and other jetting parameters (voltage of the nozzles, jetting temperature, meniscus pressure, number of jets to use, and cleaning cycles at the start/during the print operation) were tuned and saved for future use. Figure 14 exemplifies the adjustment environment of the jetting of an ink (Ink#2).

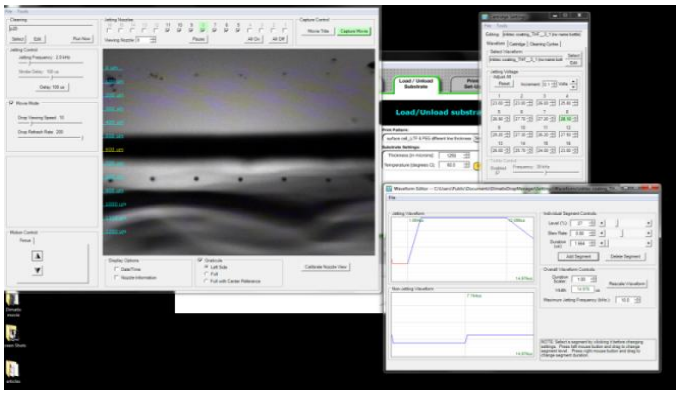

Figure 14: Screenshot showing the drop formation parameters with the drop watching camera view, taken while jetting an ink. Note that spherical drops were ejected at ~8 ms^{-1} velocity.

4.4 Jetting the Inks

Ink#1 was jetted at a 32°C cartridge temperature and at 4 inches water meniscus pressure, with the cartridge kept at a height of 0.5 mm from the substrate. A cleaning cycle of 1 sec purging and 1 sec

blotting was utilized in all the printing. The drops were jetted at a maximum jetting frequency of 5 kHz, while the velocity was maintained at between 5-7 ms^{-1}. The best jetting performances were achieved with the single firing cycle of 12.3 µs with the 4-segment jetting waveform, with the non-jetting waveform maintained at 60% voltage (see figure 15a). At segment 1 of the jetting waveform, 7% voltage with a slew-rate of 0.8 was applied for 3.3 µs while at segment 2, 100% voltage was applied for 4.8 µs with a slew-rate of 0.38. At segment 3 and 4, 60% voltage was applied for about 4.2 µs so that the operating nozzle could initiate the next cycle. Likewise, Ink#2 was jetted at the same meniscus pressure and the same cleaning cycle was maintained, though the cartridge temperature was 30°C and the cartridge height was 0.25 mm from the substrate. The maximum jetting frequency was 2 kHz with the velocity maintained at between 5-7 ms^{-1}. In this case, the single firing cycle duration was 14.9 µs, as can be seen by figure 15b. The best performances were achieved by using a 3-segment jetting waveform while the non-jetting waveform was maintained at 47% voltage. It should be noted that in the case of both the inks, the applied voltage and the slew-rate were almost identical in segment 1 as well as in segment 2, but the durations were not. For Ink#2, the duration in segment 1 was about 6 times lower than that of Ink#1 but it was double in segment 2. This implies that Ink#1 needed more time to refill the ink chamber but fired faster, while Ink#2 filled the chamber quickly but needed more pressure to fire. Also, Ink#2 required more time to complete a firing cycle: about 2.6 µs more than that of Ink#1.

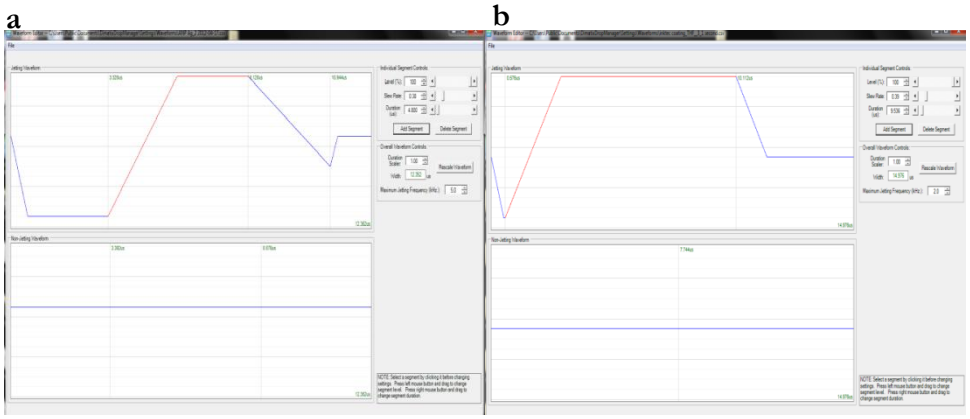

Figure 15: Adjusted jetting and non-jetting waveforms of a) Ink#1 and b) Ink#2; the highlighted part of the curves are the firing segments (segment 2). Note that the duration of the firing segment in Ink#2 is double to that of Ink#1.

After adjusting the waveform, the print resolution was needed to be fixed before any pattern could be printed. The drop size was determined by printing the test pattern and measuring the drop size using the fiducial camera and the on-screen distance measuring feature, as exemplified by figure 16a. The measured drop-size was inserted in the print pattern window and the corresponding head angle was set manually. Some patterns, a single line for example, were printed and the features were inspected carefully. Since the errors due to the radius measurement and head angle setting were unavoidable, this procedure was followed unless a satisfactory performance was achieved. Examples of these trails are illustrated in figures 11 and 12. Figure 16b shows the narrowest-line that could be achieved without any waviness and segmentation. The minimum width achieved by Ink#1, at a 6.8° head angle and 30 µm drop-radius, was 50 µm with a resolution of ~850 dpi. On the other hand, the

minimum width achieved by Ink#2, at a 5.6° head angle and a 25 μm drop-radius, was the same as that of Ink#1 but with a slightly higher resolution, ~1000 dpi.

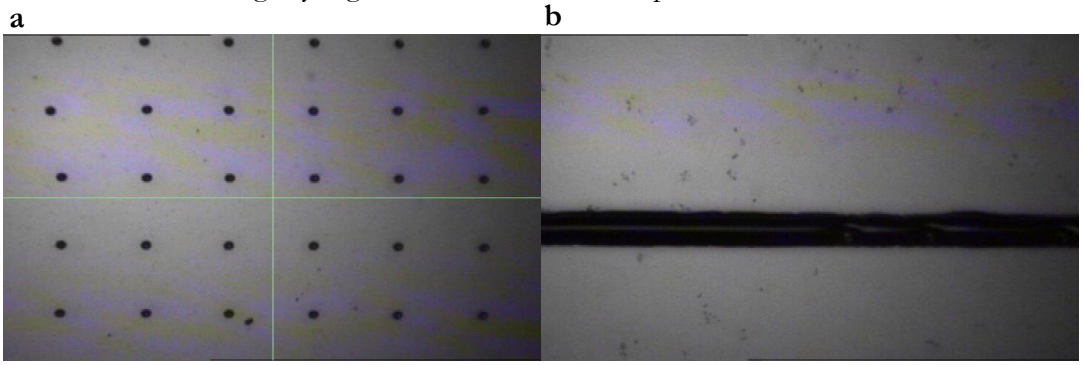

Figure 16: Print resolution experiment of Ink#1 on the glass substrate where a) drops of ink#1 on the glass substrate are seen (captured by the fiducial camera) b) 50 μm line-width (the minimum) was achieved with Ink#1. Note that the photos were taken before sintering. Also note the line-width mentioned here is the width that was inserted in the pattern editor window.

Since the inks and the printing environment may show a slight variation from time to time, the jetting performances of both inks were checked before performing any print operation; and if deemed necessary, the printing parameters and waveforms were recalibrated to restore adequate jetting performance. The user may choose any number of consecutive nozzles to perform the print operation as long as the velocities of the drops formed at different nozzles are similar (see figure 8b or figure 14). In case of these inks, though the waveforms were adjusted using a row of nozzles, only one nozzle was actually employed for the print operation. This pragmatic approach allowed for the unique opportunity to watch only a single drop formation and a very swift waveform recalibration, and importantly, this approach offered the opportunity to get rid of the unavoidable mechanical error due to a manually-set head-angle. This one-nozzle approach does however suffer greatly for more complex patterns as the printing time will be prolonged.

4.5 Sintering Ag Inks on Glass Substrates

Microscopic glass slides (Thermo Scientific, Menzel-Gläser, Germany) with a size of 76 mm x 26 mm x 0.25 mm were used as substrates. A piece of A4-size paper was placed underneath the glass slides to cover all holes in the vacuum platen. In order to have the surface smooth and clean and to enhance the adhesion angle between the surface and the fluid, the substrates were UV-ozone treated for 10 min, particles removed by a pressurized air-gun, and then wiped by a piece of cloth before being placed on the platen. The platen was kept at ~60°C for both inks. This was done for Ink#1 as it was observed that the line breaking due to the beading effect is less pronounced at ~60°C than at room temperature. On the other hand, for Ink#2, keeping the platen at ~60°C helped THF to evaporate very fast as it impinges on the platen. Immediately after the printing operation, the glass substrates were placed on a hot plate and the printed traces were sintered in air at an elevated temperature. Ink#1 was sintered at ~180°C for more than 45 min and Ink#2 was sintered at ~120°C for 15 min. In case of Ink#1, the ligands (e.g. thiols, polyelectrolytes, polymers, or polyethylene glycol) and Ag-particles are bonded together. When the heat is applied, the solvent

evaporates and the particle-ligand bonds are broken. This leads to a direct physical contact between the Ag-particles. High conductivity is achieved after sintering through the formation of percolation channels, rather than through the complete collapse of the nanoparticles into bulk metal.[21] The sintering process for Ink#2 is different. Ink#2 is a transparent, 'non-particle-type' ink and the organic dispersant of this ink is designed so that it remains in the liquid phase as a coating of the Ag-particle; but when heat is applied, the organic components and solvents evaporate. The Ag-particles sinter at the edges, so that a continuous metallic layer can form.[22, 23]

The sintering processes were observed in both cases. The temperature of the hot plate was increased gradually from 60°C to either ~180°C (Ink#1) or ~120°C (Ink#2). In case of Ink#1, the 'beading effect' was observed as soon as the drops were deposited on the glass substrate and ash-black traces were seen while the printing operation was going on. When the substrate was placed on the hot plate and the temperature was raised gradually, the printed traces remained the same throughout the observation period with no visual difference observed, i.e. the ash-black traces did not change appearance during the sintering process. On the other hand, the traces made by Ink#2 demonstrated an interesting feature, where a transition from 'liquid transparent traces' to 'non-transparent solid metallic traces' took place, as shown in figure 17. The printed traces were not visible at the time of the printing (at ~60°C), though 'liquid transparent traces' on the glass substrate could be detected after printing if the substrate was inspected at a close distance (see figure 17a). When the substrate was placed on a hot plate and the temperature was raised gradually, the traces appeared first as black lines (see figure 17b-c), and then the formation of the Ag-layer was observed as metallic silver with a slight yellow tint (see figure 17d).

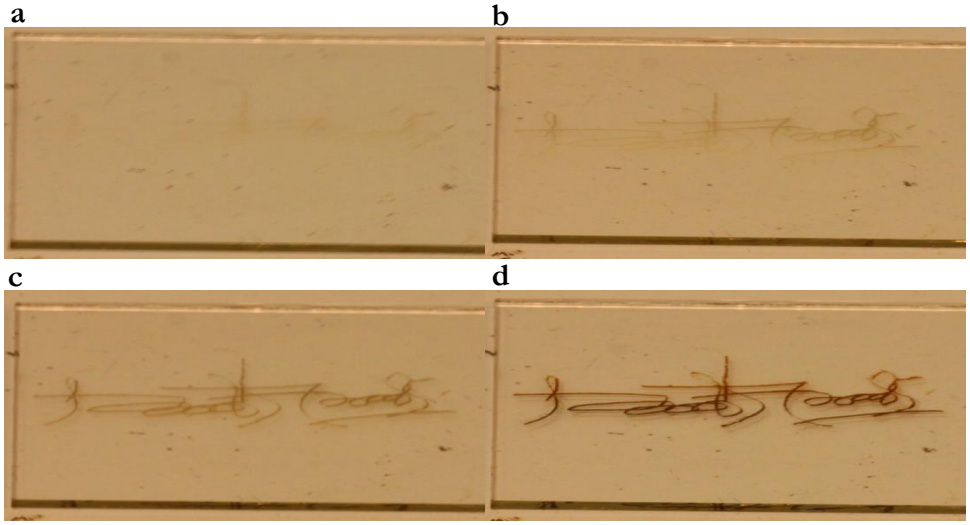

Figure 17: Photographs of Ink#2-printed traces when sintered for more than 15 min, taken at different temperatures: a) at ~60°C, b) at ~90°C, c) at ~100°C and d) at ~120°C. In addition, this complex feature exemplifies the fact that Ink#2 was optimized properly.

5 Ink Characterization

Characterizations of the inks were performed at room temperature and ambient pressure following the heat-induced sintering, during which the inks had formed conductive Ag-traces on the glass substrate. These characterizations encompass specific resistance measurement and thickness measurement of the printed traces. In addition, the physical appearance of the liquid Ag-inks when stored in air was also observed.

5.1 Theory: Specific Resistance Measurement

Ohm's law states $V=IR$, where I is the current between two points of a conductor, V is the voltage difference between the two points, and R is the resistance. If the temperature is kept fixed, the resistance R of a 3-dimensional Ohmic conductor depends on the dimensions only i.e. $R \propto \frac{L}{A}$, where L is the length and A is the cross-section area, being the product of the width W and the thickness, t (i.e. $A=Wt$), as illustrated by the schematic in figure 18. The proportionality constant of this relation is called the specific resistance ϱ. This is an intrinsic property of a material that only depends on temperature. For pure metallic Ag at 20°C, the specific resistance is ϱ =1.59 μΩ-cm (i.e. ϱ =1.59*10^{-8} Ω-m). Using the equation, $R=\frac{\rho L}{A}$, the specific resistance of the material can be obtained by measuring the resistance R of a 3-dimensional sample and plotting it as a function of L/A. The slope of this plot will be the specific resistance ϱ.

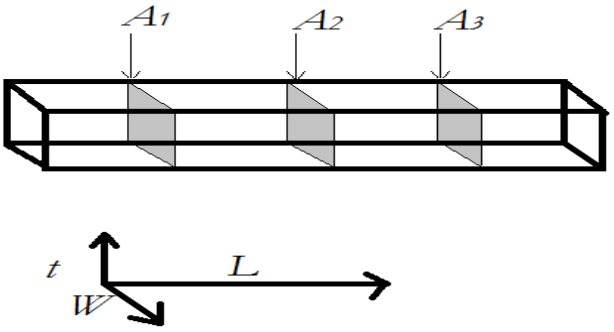

Figure 18: Schematic of the 3-dimensional arrangement of a sample.

5.2 Experimental setup and Measurement Conditions

Though a 4-point probe instrument could be used to measure the sheet resistance of the printed Ag films directly, a different procedure was employed in this thesis, as a 4-point instrument may easily scratch the printed films on the glass substrate. The 4-point probe technique further requires a 'uniform surface' of specific area which is quite impractical for the jetted inks since a larger area may result in a non-uniform surface after sintering. Therefore, to measure the specific resistance of the Ag-traces on the glass substrates, a new set of two pair of probes was designed (see figure 19b), so that a constant current could be applied through one pair of probes, while the resulting voltage at the sample contact-points was measured with the other pair of probes. However, the new probes act independent of each other, and the distance between them cannot be determined with great

accuracy. Determining the sheet resistance of a film directly using the new probes is therefore difficult. However, they are very useful for determining the resistance of thin lines.

The probes were connected to an Agilent 34401A digital multi-meter (Agilent technologies Inc., USA), and a LabView® program (National Instruments Corp., USA) was designed (see figure 19c-d) to control the resistance measuring setup. All samples (see figure 19a) were fabricated with only one print sweep. Extra drops were deposited manually using a syringe at the end points of a trace after printing (but before sintering) in order to facilitate the connection between the sample and the probes. Three lengths were printed with each ink: L = 2 cm, L = 3 cm and L = 4 cm. Each sample-length was printed in 10 different widths: from 50 μm to 1 mm. Hence a total of 60 samples (3 x 10 x 2 = 60) were prepared, as can be seen by figure 19a. Each sample was characterized with the aforementioned LabView-Agilent-probe setup. 20-25 readings were recorded for each sample, and the average was used as the effective resistance R of a single sample. Though L and W were defined in the pattern editor window before printing and be deposited on the glass substrate almost with the same dimensional precision, variations were observed due to variations of the drop-size, waviness of the printed traces, the adhesion between glass-ink pairs, and the sintering mechanisms. To circumvent these variations, several cross-sectional surface profiles were measured at different points of each sample (see figure 18) using the DektakXT Stylus Surface Profiling System (Bruker Corp., USA), as shown in figure 19e-f. These surface profiles were exported to Origin® 8.5 (OriginLab Corp., USA), where the areas under each profile curve could be calculated. The non-ideal trace was then modeled by a perfect straight rod, with a cross sectional area A given by the average of several surface-profile areas. Finally, all R and A values for a specific L were plotted on an 'R versus L/A' graph using Origin® 8.5. A linear fitting of the slope of the plotted data gave the specific resistance ϱ. Thus, three specific resistances for the different L values were obtained for each of the inks. In addition, the average thickness t was obtained using the DektakXT, Stylus Surface Profiling System, and the physical appearances of the Ag-inks were observed for over a month under ambient conditions and duly documented.

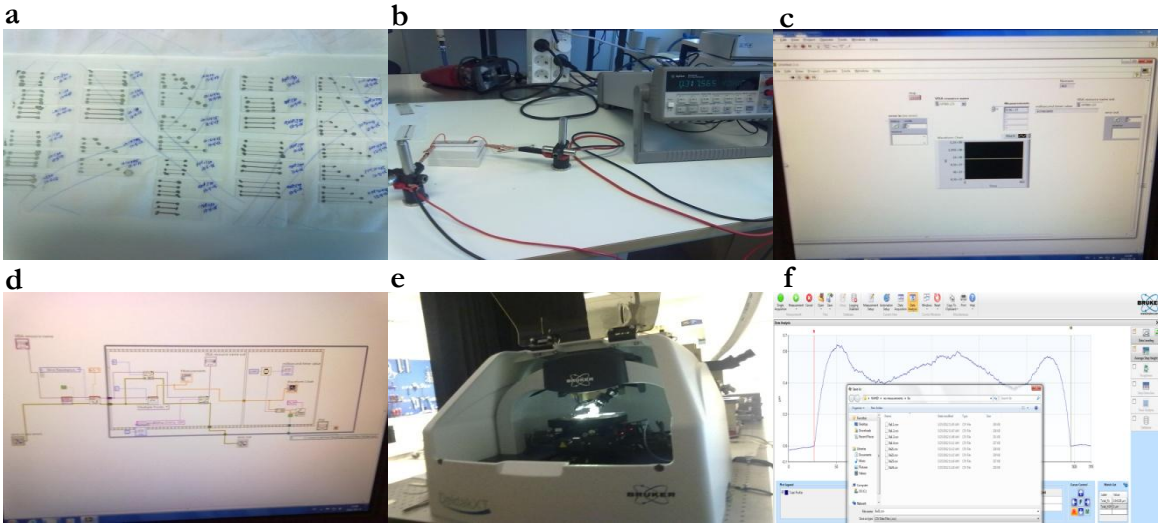

Figure 19: Characterization experiment, showing a) samples printed on the glass substrate after sintering, b) designed probes, c) front-panel, and d) back-panel of the designed LabView® program, e) DektakXT, Stylus Surface Profiling System (Bruker Corp., USA) and f) the surface profile acquired by the profilometer.

5.3 Results and Discussions

The specific resistances at different L obtained for Ink#1 and Ink#2 are shown in figure 20. The measured specific resistance of Ink#1 falls in the range of 10-19 μΩ-cm, and for Ink#2 in the range of 5.4-13.8 μΩ-cm. In comparison with the specific resistance of bulk Ag (1.59 μΩ-cm at 20°C), Ink#1 shows 6-10 times higher sp. resistance while Ink#2 shows 4-8 times higher sp. resistance. The manufacturers claim that the specific resistance of the Ag-traces (after sintering) to be 5-9 μΩ-cm and 6 μΩ-cm, respectively, close to what is observed.

The difference between the measured values and the vendor specified value might be a measurement artifact: due to the manually deposited drops at the ends of each line that may increase the length L (see figure 19a), due to the positioning of the two points at the profilometer that may overestimate the width W (see figure 19f), and due to insufficient data points in the linear fitting (see figure 20a-f).

The thickness of the traces printed by Ink#1 spans a range of 0.3-0.5 μm (i.e. 300-500 nm), and for Ink#2 the range is 0.08-0.1 μm (i.e. 80-100 nm). The average thickness of Ink#1-printed traces is thus ~4 times higher than that of Ink#2, as indicated further by the difference in colors in the respective 3D scans, shown in figure 21b and 21d. A hypothesis is that when THF was mixed with Ink#2 in a ratio of Ink#2: THF=3:1, the Ag content lowers to ~7.5 wt% from the original (10 wt%), which results in ~4 times lower Ag content than Ink#1. Also, the print-resolutions of both the inks are almost the same, which signifies the fact that the drops jetted with the inks are almost identical in volume. Hence, it can be approximated that having ~4 times higher Ag content than Ink#2, Ink#1 results in ~4 times thicker traces than its counterpart. In addition, it was observed that the peak thickness of Ink#1-printed profiles is at least twice that of Ink#2-printed profiles, as evidenced by figures 21a and 21c that show the peak-values of the respective profiles as obtained by the profilometer. The peak thickness of each profile was taken into particular consideration, because sandwich cell LECs suffer from the possibility of experiencing shorts in between the electrodes, with a more uneven line being more sensitive to short circuits than an even line.

Furthermore, the physical appearences of the inks were observed. Though Ink#1 did not show any change in its appearance, Ink#2 demonstrated an interesting property as it changed its liquid appearance from clear-transparent to red-brown during the first week of storage. It continues to change to a darker reddish up to 3-4 weeks, and therafter return to a clear transparent state after 5-6 weeks, as shown in figure 22. Since the detail of the ingredients of the ink is unknown, the reason behind this appearance-change is difficult to pinpoint. Though no precipitation was observed, there may be an interaction with light that results in the change of appearance. This hypothesis is supported by the fact that the manufacturer supplied the ink in a black-plastic bottle, as shown previously in figure 13a. To improve repeatability, all the printing operations discussed in this thesis

were performed with 'fresh' inks. No experiment was performed to characterize how inkjetted traces are influenced by this appearance-change.

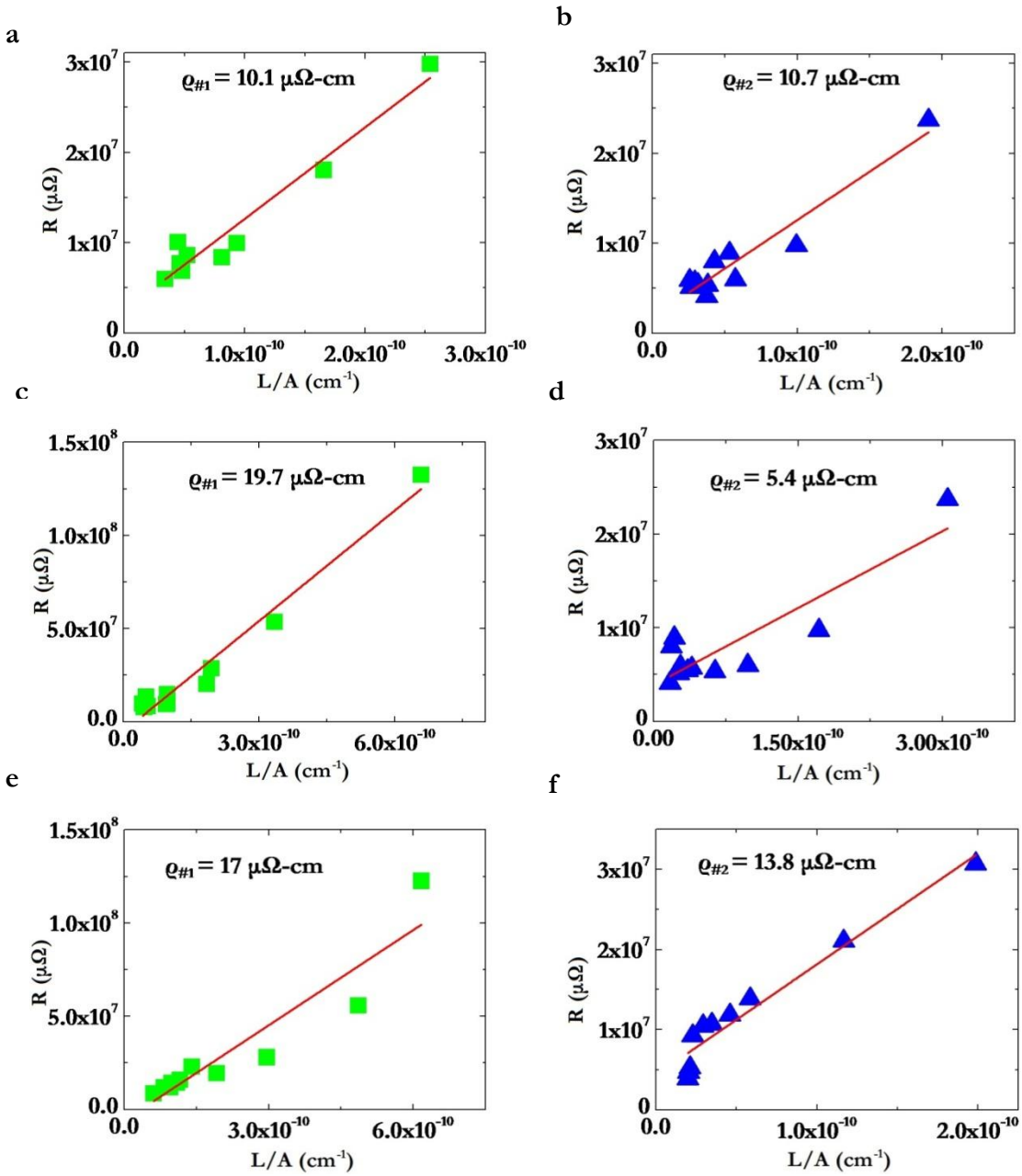

Figure 20: Specific resistance measurement plots: 'R versus L/A', showing the specific resistances of Ink#1 (20a, 20c, 20e) and Ink#2 (20b, 20d, 20f) for the three lengths: (a-b) L=2 cm, (c-d) L=3 cm and (e-f) L=4 cm, respectively.

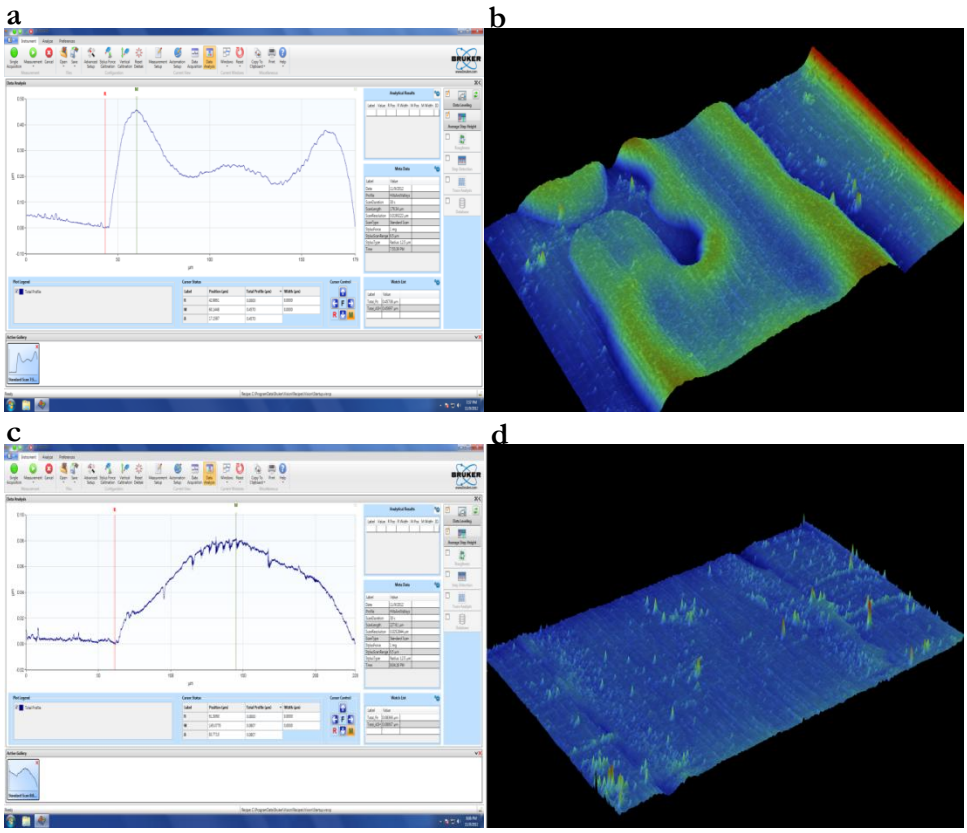

Figure 21: Surface profiles and 3D photos of a-b) Ink#1-printed and c-d)Ink#2-printed traces. Note that the color differences in the 3D photos (figure 21b-d) are due to the thickness of the traces, illustrating the fact that Ink#1 trace is thicker than that of Ink#2.

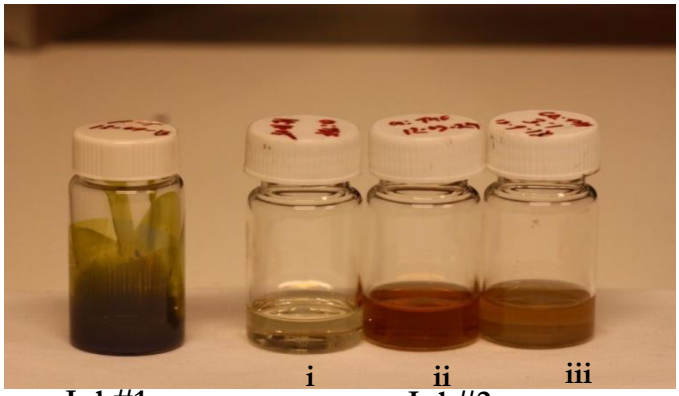

Figure 22: Physical appearances of the inks. Ink#1 displays no change after being stored in air for 4 weeks, while Ink#2 demonstrates a distinct shift of its color: i) 'fresh', ii) after 2 weeks, and iii) after 4 weeks.

6 Performance in LECs

The primary objective of this thesis-work was to find an inkjet compatible Ag-ink that is functional as an electrode in a LEC. Though performance can be measured in terms of specific resistance, as discussed in the previous sections, compatibility of the inks with the electrochemical nature of the LEC is essential. Additives in the inks, about which nothing is known, might react during the reduction and oxidation of the LEC and might result in poor, or no, light emission. In order to compare the two inks, it is therefore essential that their performances as electrodes in the sandwich-cell structured LECs are measured.

6.1 Theory: Working Principal of LECs

In order to understand the working principal of LECs, the analogous description of its doped inorganic semiconductor device counterpart is helpful to start with. Simply put, when an external voltage is applied, holes/electrons are injected at the anode/cathode, a process that is facilitated by placing a p-doped material next to the anode, and an n-doped material next to the cathode. The interface between the p-doped and the n-doped regions is called a p-n junction, and here electrons and holes can recombine under the formation of excitons. The decay of the excitons can result in the emission of radiation. If the frequency of this radiation, which depends on the energy gap between the conduction band and the valance band of the material, falls within the visible region, the radiation is seen as light. Thanks to the π-conjugated polymer theory, conjugated polymers, polyacetylene for example, operate analogously. Though a polymer is typically a non-crystalline, three-dimensional entity composed of chains with finite length which results in an energy band scheme that is essentially very complex, one can still approximate it with a material having a valance and conduction band. In organic electronics, the collection of energy levels corresponding to the top of the valance band is referred to as HOMO and the bottom of the conduction band is referred to as LUMO. This comparison is illustrated by the schematics shown in figures 23a and 23b. These polymers, when powered by an external power supply, can emit light through the recombination of electrons in the LUMO and holes in the HOMO. Like inorganic semiconductors, the polymers' electrical properties can be manipulated by doping, for example, by chemical reduction/oxidation using a redox agent, or through electrochemistry by adding an electrolyte so that electrons/holes are added to the LUMO/HOMO bands and subsequently subjecting the polymer-electrolyte mix to a potential bias.[24, 25]

In the basic configuration of the LEC, the semiconducting polymer and the electrolyte, hereafter referred to as the active material, are sandwiched between two electrodes, as shown in the schematic of figure 23. Figure 23b illustrates what happens in the absence of an external power supply. The energy bands i.e. LUMO and HOMO are not subjected to any voltage bias and are therefore illustrated as flat lines. In this state, no charge injection takes place since the HOMO is filled and electrons do not have enough energy to reach the LUMO. Immediately after applying a potential bias, as indicated by the inclined lines of the LUMO and HOMO of figure 23c, no significant injection of electrons/holes occur as the energy barrier is still too large for efficient tunneling, assuming that all the active material is subjected to a constant potential gradient. However, the applied potential allows for ion migration throughout the active material, pushing positively charged

ions towards the cathode and negatively charged ions towards the anode. Gradually, these ions will screen the electrostatic potential from the electrodes, and eventually form electrical double layers in the vicinity of the electrodes, as shown in figure 23d. Hence, the width of the energy barriers between the electrode and the active material decreases, which enables significant electron/hole injection into LUMO/HOMO by tunneling, as shown in figure 23e. These injected and subsequently charge-compensated electrons and holes reduce and oxidize the polymer, respectively, which in turn results in a significant increase of the conductivity of the active material. These electrochemical doping progresses continue until the two doping fronts meet in the center region under the formation of a p-n junction, as shown in figure 23f. It is at the p-n junction that light is created.

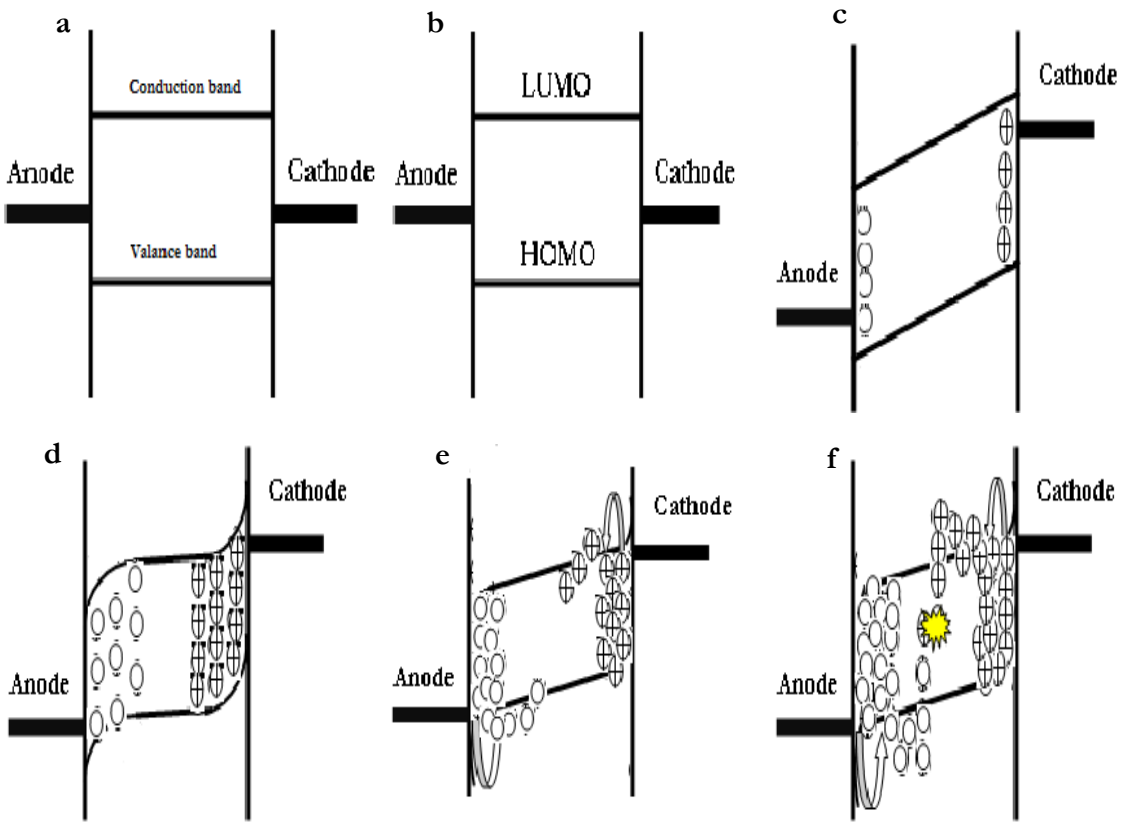

Figure 23: Schematics, illustrating the working principal of the LEC at different states.

6.2 Making Sandwich-cell Structured LECs

The sandwich-cell LEC was made according to the schematic shown in figure 24. The active material was sandwiched between printed Ag-electrodes on a glass substrate, and a thermally evaporated Al-film.

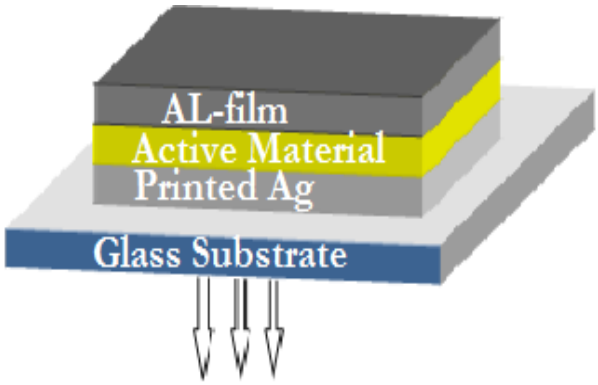

Figure 24: Schematic of sandwich-cell structured LEC.

6.2.1 Printing the Bottom Electrodes

The bottom electrode of the sandwich-cell LEC was printed on the UV-ozone treated clean glass substrates in the same fashion as described in the previous sections. To compare the performance of the two inks, the structure of the LEC was kept fairly simple. Two lines with the same dimensions were printed side-by-side, using ink #1 for line 1 and ink #2 for line 2. Hereafter, this arrangement will be referred to as 'electrode pair'. Several samples of electrode pairs can be seen in figure 25a and 25c. In order to print the bottom electrodes, a 20 mm long and 70 μm wide line was printed and sintered with Ink#2. After that, Ink#1 was used to print another line of the same length and width parallel to the first one on the same substrate, at a distance of 2-3 mm from the first one. Since it was observed that Ink#2 can withstand a 180°C temperature without any influence on the conductivity, this extra curing of Ink#2 was assumed to not affect the results. As can be seen in figures 25a and 25c, these two printed lines were connected together using syringe-deposited drops and conductive tape to facilitate the use of the measuring probes. This is further demonstrated in figure 26 and 27a where it can be seen that an electrode pair is connected with the external probes by the means of the conductive tape.

6.2.2 Preparing the Active Material and Drop-casting

The active material solution comprised Superyellow (SY, Merck, PDY-132), poly(ethylene glycol) dimethacrylate (PEG-DMA, Sigma Aldrich) and potassium trifluoromethanesulfonate (KCF_3SO_3, Sigma Aldrich). SY was dissolved in toluene by using a magnetic stirrer and an elevated temperature of 50°C (323 K) for 24 hours while PEG-DMA and KCF_3SO_3 were dissolved in cyclohexanone. Dissolving and mixing the materials was performed under ambient conditions, and all solutions were made using a solid material content concentration of 10 mg/ml. These solutions were mixed in a mass ratio of SY:PEG-DMA:KCF_3SO_3=1:0.5:0.1 that resulted in the desired active material; a glass vial that contains the blended active material as can be seen in figure 25b. Spin-coating of the active material at a rate as low as 800 rpm (for 60 sec) was tested (and yielded films with an average

thickness of 0.15-0.2 μm), but unfortunately was found to regularly result in shorts between the Al-film and the printed Ag-lines, as exemplified by figure 26. Hence, drop casting of the active material solution was tested instead, as depicted in figure 25b. A glass pipette was used to drop-cast the active material onto the printed electrodes. The glass substrate was placed on a flat surface and the active material was deposited with the pipette-made drops by moving over the substrate from one side to another in a slow manner, and returning to the beginning for the next sweep. 3-4 sweeps were needed for each substrate. Since the aim of this process is to have a film as uniform as possible, the velocity of the sweeping motion over the substrate was maintained constant. In addition, the process was performed very carefully so that all the samples on a substrate were covered, but no drops were deposited out of the substrate, as evidenced by figure 25c. Also, whenever an air-bubble was formed, it was removed using the pipette. After completing the drop-casting, the substrate was dried for 15-20 min in air before it was mounted onto a shadow-mask (see figure 25d). Figure 25c shows the drop-casted material during drying. The material dried first at the edges of the substrate, as indicated by a color shift. The center of the substrate remained wet for the longest period. The average thickness of the drop-casted layer was measured with the surface profile and found to be 0.3-0.4 μm.

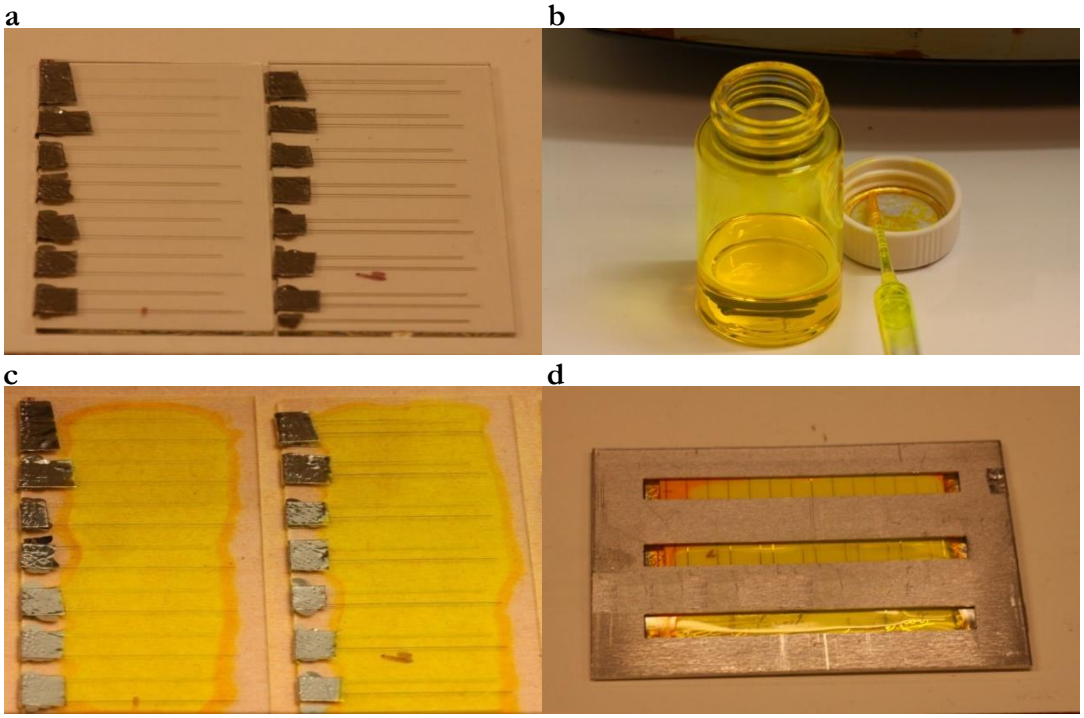

Figure 25: The fabrication of sandwich-cell LECs with printed electrodes showing a) electrode pairs on glass substrates, b) active material ink in a material mass ratio of SY: PEG: KTF=1:0.5:0.1, c) drop-casted active material on top of the electrode pairs and d) samples mounted with the shadow-mask so that an evaporated Al-film can be made with dimensions defined by the shadow-mask.

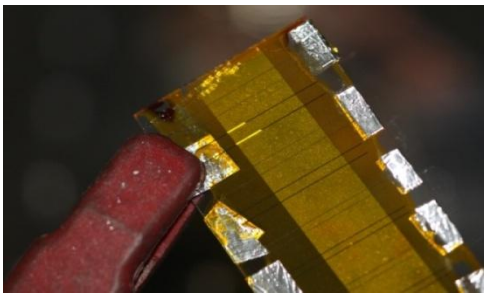

Figure 26: An electrode pair of LECs experiencing shorts between the Al-film and the printed Ag-lines when the active material was spin-coated.

6.2.3 Drying the Active Material and Evaporating the Top Electrode

After mounting the samples on the shadow mask, the arrangement was transferred to a hotplate set to ~70°C, and left to dry for 14-15 hours. This drying was performed inside a glove box with nitrogen atmosphere containing less than 1 ppm oxygen and water; hereafter referred to as the 'wet box'. After drying, the samples were transferred to a thermal evaporation chamber (Univex 350, Oerlikon, Leybold Vacuum, Germany) positioned in another glove box, also filled with nitrogen atmosphere but completely solvent free; hereafter referred to as the 'dry box'. In the evaporation chamber, an Al-film was deposited (Al, 99.999%, Umicore) on top of the active material, with a 76 mm x 9 mm area defined by the shadow mask (see figure 25d). The thickness of Al-film was controlled to 0.09-0.1 μm. The active material is now sandwiched between the Ag-printed bottom electrode and the Al top electrode.

6.3 Experimental Setup and Measurement Conditions

Thanks to the open structure of the printed Ag-traces, light from the LEC can escape through the Al electrodes and the glass substrate, in the direction of the arrows shown in the schematic of figure 24. The electrode pair was tested right away in the dry box while applying a voltage bias between the printed Ag-electrode and the evaporated Al-electrode. Since both the electrodes in the electrode pair were connected, both of them experienced the same voltage bias. The only difference between the two LECs is the ink from which the Ag electrodes were fabricated, and consequently it is straightforward to attribute observed differences in turn-on time, brightness etc. to the ink selection.

A Keithley-4200 Semiconductor Characterization System (Keithley Instruments Inc., USA) was used to apply a constant voltage of 5 V and to measure the current as a function of time. The probes (Signatone, CA) inside the dry box were connected to the Ag-and Al-electrodes. The light emission was documented by taking photos with a camera (Canon EOS 50D) equipped with a macrolens (Canon Macro Photo Lens MP-E 65 mm 1: 2.8) placed inside the dry box, by maintaining the same settings (f/4, 3 sec exposure time, ISO-3200, 65 mm focal length) during the whole experiment. The photographs were taken consistently as the experiment was carried out, using the camera controlling-software DSLR Remote Pro-Remote Capture Application for Canon EOS Digital S. Since the exposure time of the camera was 3 sec, the timing may suffer an error but it had almost no effect on the study.

6.4 Results and Discussions

The experimental set-up is shown in Figure 27a. Figure 27b demonstrates an electrode pair as a reference where Ink#1 and Ink#2 are indicated clearly; all the following pictures in this section are presented in this order.

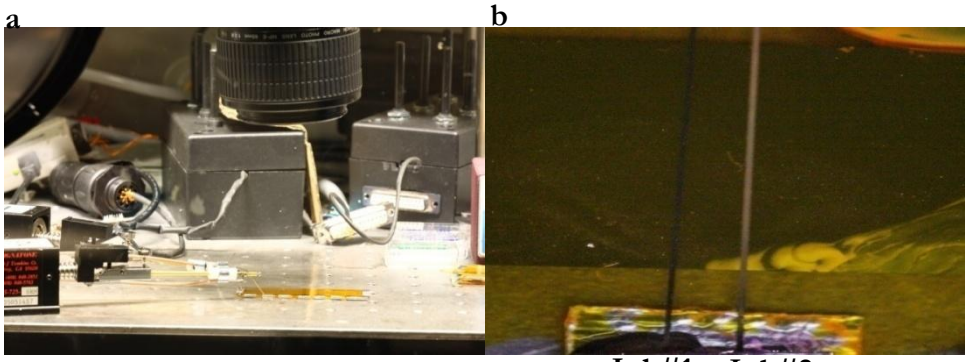

Figure 27: Performance comparison experiment, showing a) experiment setup in the dry box and b) two Ag-traces in an electrode pair configuration as seen from the opposite side of the glass substrate. Note the difference in color of the printed lines. Electrodes printed with Ink#1 are darker than those printed with Ink#2.

First, performance comparisons regarding the turn-on time of the LECs were conducted. Here, 0 sec refers to the time when a constant voltage bias (5 V) was applied to the electrode pair. The turn-on time is defined as the time at which visible light could be seen with the above mentioned settings of the camera. Figure 28 signifies the turn-on time of both the LECs where it can be seen clearly that the turn-on time differs with about 40 sec (see figure 28a-b). Ink#1 LECs are slower to turn on compared to Ink#2 LECs. A careful inspection of figure 28a-b shows that Ink#2 starts 'glowing' at 10 sec while Ink#1 needs at least 50 sec.

Second, performance comparisons regarding the brightness of the LECs were conducted. Referring to all the data presented in figure 28, it can be seen that the light coming out from Ink#2 LECs is brighter than its Ink#1 counterpart. A careful inspection of figure 28e-f shows that at ~200 sec, almost all the areas of Ink#1 LEC emitted light but with less brightness than the Ink#2 LEC.

Third, performance comparisons regarding the color/appearance of the printed traces were conducted. Referring to figure 28, it can be seen that the light comes out from both sides of the electrodes, as seen by the Ink#2 LEC in figure 28b. However, because of the brightness, it seems that the light is emitted as single line, as seen by the Ink#2 LEC in figure 28d. In contrast, a careful inspection shows that Ink#1 LECs never demonstrate such an appearance of single-line emission. This indicates that Ink#2 LECs are brighter than Ink#1-made LECs, and that the concept of solid silver traces as semi-transparent electrodes could work in a homogenous light emitting device. The hypotheses are that the wider the electrodes, more of the light is blocked in this particular configuration of the LEC, and the colors/appearances of the electrodes help/hinder the light in exiting the device. In the case of Ink#1, the 'ash-black' and 'absorbent' appearance of the electrode (see figure 27b) hinders the light to come out while in the case of Ink#2, its appearance became

advantageous; the 'silver-like' and 'semi-transparent' appearance of the electrode helps the light to escape the device, as evidenced by figure 28.

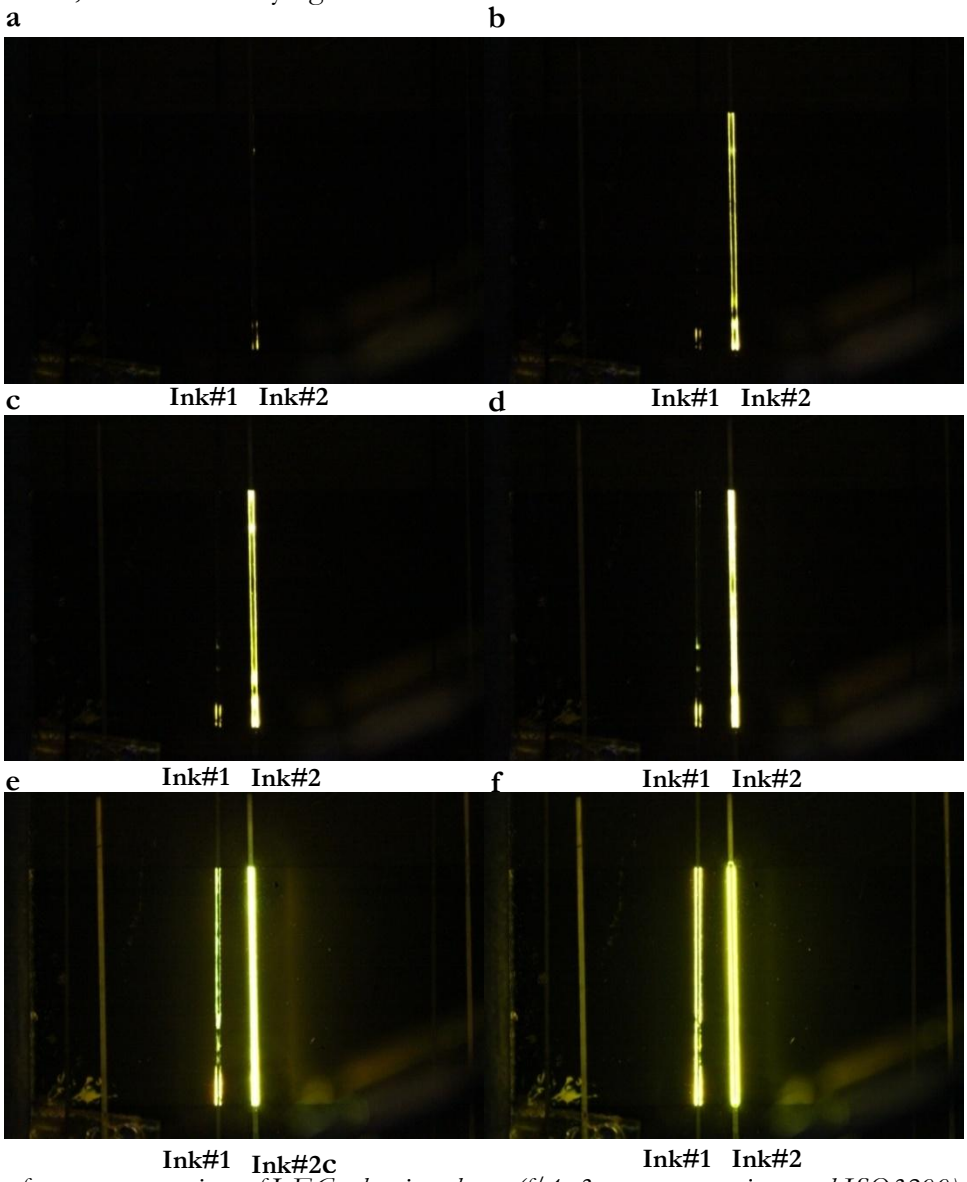

Figure 28: Performance comparison of LECs showing photos (f/4, 3 sec exposure time, and ISO3200) taken at a) 10 sec, b) 50 sec, c) 100 sec, d) 150 sec, e) 200 sec, and f) 300 sec.

Fourth, it was observed that in some cases, Ink#1 LECs did not emit light at all while Ink#2 LECs demonstrated the expected emission. Figure 28 illustrates this fact; though both the LECs comprises to the same electrode pair, Ink#1 LEC did not emit any light whereas the Ink#2 LECs did. The hypotheses are that the electrode printed with Ink#1 could be broken so that it was not a functional device at all, and the thickness of the electrode printed with Ink#1 is too large for this particular configuration of LECs. This later fact implies that the drop volume of Ink#1 is so big that the printed line protrudes through the active material layer to make direct contact with the Al-film. The thickness measurement provides indications in support of this hypothesis since the measurement showed that the average printed thickness of Ink#1 is ~4 times greater than that of Ink#2. Also,

when the largest thicknesses of the respective ink-profiles were considered, it came out that Ink#1 is at least twice as thick as its counterpart. Consequently, this raises the possibility of making direct contact, i.e. a short circuit, with the top electrode in the sandwich-cell configuration.

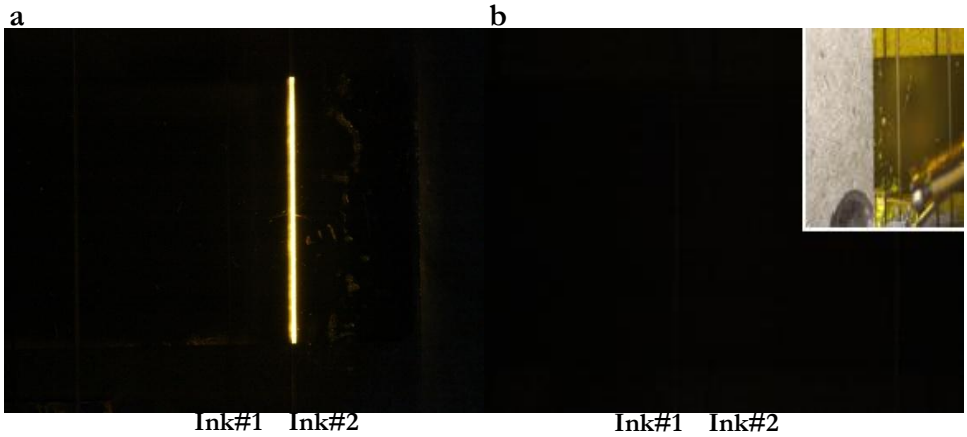

Figure 29: Electrode pair demonstrating a) an Ink#2 LEC shining while the Ink#1 LEC is not working at all and b) none of the LECs are shining. Inset of 29b shows the electrode pair under illumination. Note that throughout the course of these experiments, it was never observed that an Ink#1 LEC emitted light while an Ink#2 LEC did not.

Fifth, performance comparisons regarding the Ag content of the inks were conducted. Referring to figure 29, it can be seen that solely the Ink#2 LEC is emitting light (see figure 29a) or that none of the LECs in an electrode pair are emitting (figure 29b). In performing the experiments, it was observed that the Ink#2 LECs always demonstrated light emission when an electrode pair was working. In contrast, it was never observed that an Ink#1 LEC was emitting while an Ink#2 LEC did not. The hypotheses are that the electrode pair was not made properly, the active material was not drop-casted properly, breaking off/scratching of the devices may happen during handling etc. When only Ink#2 LECs are emitting but not Ink#1 LEC, the most probable explanation is the thickness. Ink#1 electrodes are thicker than Ink#2 electrodes, as its ink consists of ~30% Ag particles which results in rigid and filled traces after sintering. In comparison, Ink#2 consists of 10% Ag particles and the printed traces are accordingly less thick than its counterpart. In the case of this particular configuration of the LEC, Ink#1 shows more possibility in protruding through the active material layer than Ink#2, even when drop-casting, as evidenced by figure 29. Hence, the data indicates that a higher loading of Ag particles could be a disadvantage that ultimately diminishes the performance of the LEC, particularly in the case of the sandwich-cell configuration.

7 Comparison at a Glance

This section covers the comparison between the Ag-inks at a glance. The following table summarizes all the specifics about the inks as they were studied in this thesis.

Issues	Ink#1	Ink#2
Jetting temperature, meniscus pressure	32˚C, 4 inch-water	30˚C, 4 inch-water
Max. jetting frequency (kHz) (using 10 pl cartridge)	5	2
Jetting velocity (ms^{-1})	5-7	5-7
Single firing-cycle (µs)	12.3	14.9
Drop-size (µm), Head-angle, resolution (dpi)	30, 6.8˚, 850 (approx.)	25, 5.6˚, 1000 (approx.)
Min. line-width (µm)	50	50
Substrate temperature (while jetting)	60˚C	60˚C
Sintering condition	~180°C, more than 45 min in ambient	~120°C, more than 15 min in ambient
Appearance change while sintering	No change	liquid transparent phase to solid metallic phase
Ink-appearance following 5-6 weeks storage in glass vial in ambient	No change	Water-like to reddish-brown in 3-4 weeks and to water-like again in 5-6 weeks
Measured specific resistance after sintering (µΩ-cm)	10-19	5.4-13.8
Specific resistance compared with bulk Ag (at 20˚C)	6-10 times higher	4-8 times higher
Manufacturers' claim on specific resistance after sintering (µΩ-cm)	5-9	6
Thickness on the treated glass substrate (µm)	0.3-0.5	0.08-0.1
Turn-on time (at 5 V)	Slower (~50 sec)	Faster (~10 sec)
Brightness	Less bright	Brighter
Sandwich-cell configuration: electrode's appearance on the glass substrate	Ash-black, absorbent; hinders the light to come out	Silver-like, semi-transparent; helps the light to come out
Sandwich-cell configuration: homogenous light emission	Shows less homogeneity; never appears as a single line	Shows better homogeneity; appears as a single line
Sandwich-cell configuration: possibility of making direct contacts i.e. short circuits	Demonstrates more possibility because of its higher Ag content	Demonstrates less possibility because of its lower Ag content

Table 2: Specifics about the inks and comparison at a glance.

8 Conclusion

The thesis reveals that Ink#2 is better than Ink#1, as the electrode of the sandwich-cell LEC comprising an Ink#2 bottom anode emits more light with a faster turn-on time compared to a device comprising an Ink#1 anode. Also, this work ascertains that the specific resistances of the Ag-traces printed with both the inks are only 4-10 times higher than that of bulk Ag. Most importantly, considering the high price of Ink#1, Ink#2 offers the opportunity of making printed electrodes in a highly cost-effective way.

Though the work demonstrates that both the inks can be jetted with the inkjet printer DMP-2800, Ink#2 requires a reformulation. However, the results indicate that this is possible and presents a viable method of getting satisfactory results. It is shown that Ink#2:THF = 3:1 (vol:vol) results in improved jetting performance. Though it was recommended that the solvents used for the functional fluid should have low evaporation rates with high boiling points (more than 100°C), this thesis work verifies otherwise, as evidenced by the successful jetting of an ink mixed with a highly volatile, low boiling point solvent like THF (boils at 66°C). In fact, the addition of THF is advantageous if the substrate temperature can be kept close to its boiling point, and an improved resolution of the printed features is demonstrated.

Finally, this thesis work puts a question mark on a commonly expected feature regarding the percentage of the metallic content of an ink. Is a higher metallic content always preferred? Here, it is shown that Ink#1 contains 3 times more Ag-particles and makes ~4 times thicker traces than Ink#2. However, such thick printed traces demonstrate a higher probability for short circuited devices by protruding through the active material layer, and the LECs made with this ink emit light with less homogeneity than its counterpart. Hence, this work suggests that the high metallic content ink is not the preferred choice for sandwich-cell LECs.

9 Future Prospects

As demonstrated in this work, the jetting of Ag nanoparticle-based inks with the inkjet printer provides a unique opportunity to make printed electrodes for LECs. LECs were fabricated in a sandwich-cell configuration with the bottom anodes ink-jetted in a single-line configuration. A future investigation can aim for printing electrodes with more complicated patterns using other kinds of available cartridges, which should be of interest for, e.g., large-area LEC configurations. Printing electrodes for other configuration of LECs e.g. the planar-cell configuration, can also be a possibility. As evidenced by this work, the printed electrodes can protrude through the active material, even when a thick drop-cast active layer is used. One way to avoid this problem is to spin-coat a PEDOT:PSS layer on top of the electrodes in the sandwich-cell configuration. Hence, a future experiment and comparison study could include an extra layer of PEDOT:PSS on top of the inkjetted Ag anode. The future studies could also focus on the addition of suitable additives to Ink#1 since no study was performed on this regard. In addition, the future study could encompass the study on finding the reasons behind the observed color change of Ink#2 and could look for the performance deterioration due to this change. As this thesis work did not focus on using different substrates and their treatment, investigations can also be carried out regarding the effects of the ink-substrate properties and the ideal conditions for Ag sintering. Moreover, this comparison study concludes that the reformulated Ink#2 performs well, and since this ink is much cheaper than Ink#1, working with Ink#2 is recommended. Finally, it is suggested that research should be performed on the formulation, and subsequent printing, of other conductive inks like graphite and graphene inks, conductive polymers like PEDOT:PSS[26], small-molecule light-emitters,[27] which could pave the way to the realization of a large-area LEC devices manufactured entirely by an inkjet printer.

10 Bibliography

1. A. Sandström, H. F. Dam, F. C. Krebs, and L. Edman, "Ambient fabrication of flexible and large-area organic light-emitting devices using slot-die coating," Nat Commun 3, 1002 (2012).
2. A. Sandström, P. Matyba, O. Inganäs, and L. Edman, "Separating Ion and Electron Transport: The Bilayer Light-Emitting Electrochemical Cell," Journal of the American Chemical Society 132, 6646-6647 (2010).
3. S. Tang, A. Sandström, J. Fang, and L. Edman, "A Solution-Processed Trilayer Electrochemical Device: Localizing the Light Emission for Optimized Performance," Journal of the American Chemical Society 134, 14050-14055 (2012).
4. L. Edman, D. Moses, and A. J. Heeger, "Influence of the anion on the kinetics and stability of a light-emitting electrochemical cell," Synthetic Metals 138, 441-446 (2003).
5. L. Edman, "Bringing light to solid-state electrolytes: The polymer light-emitting electrochemical cell," Electrochimica Acta 50, 3878-3885 (2005).
6. J. H. Shin, P. Matyba, N. D. Robinson, and L. Edman, "The influence of electrodes on the performance of light-emitting electrochemical cells," Electrochimica Acta 52, 6456-6462 (2007).
7. A. Asadpoordarvish, A. Sandström, S. Tang, J. Granström, and L. Edman, "Encapsulating light-emitting electrochemical cells for improved performance," Applied Physics Letters 100, 193508 (2012).
8. Pachler, P, Wenzl, P. F, Scherf, U, Leising, and G, "The Efficiency of Light-Emitting Electrochemical Cells," Journal of Physical Chemistry B 109, 6020-6024 (2005).
9. S. van Reenen, R. A. J. Janssen, and M. Kemerink, "Dynamic Processes in Sandwich Polymer Light-Emitting Electrochemical Cells," Advanced Functional Materials 22, 4547-4556 (2012).
10. A. Sandström, P. Matyba, and L. Edman, "Yellow-green light-emitting electrochemical cells with long lifetime and high efficiency," Applied Physics Letters 96, 053303 (2010).
11. Dimatix, "http://www.fujifilmusa.com/support/ServiceSupportBrowse.do?prodcat=879589&sscucatid=664271&sscucatid=664272." published by Fujifilm Dimatix Inc., USA (2012), Access date: 2012-11-20
12. Dimatix, "http://www.fujifilmusa.com/support/ServiceSupportProductContent.do?dbid=881325&prodcat=879589&sscucatid=664272." published by Fujifilm Dimatix Inc., USA (2012), Access date: 2012-11-20
13. H. Wijshoff, "The dynamics of the piezo inkjet printhead operation," Physics Reports 491, 77-177 (2010).
14. M. R. Keeling, "Ink jet printing," Physics in Technology 12, 196 (1981).
15. G. R. Maruschock, "A SYSTEM TO ANALYZE CONTINUOUS INKJET DROPLETS," in School of Engineering(University of Pittsburgh, 2004).
16. A. v. d. Bos, "AIR TRAPMENT and DROP FORMATION in PIEZO INKJET PRINTING," in Physics of Fluids(University of Twente, 2010).
17. B. Derby, "Inkjet Printing of Functional and Structural Materials: Fluid Property Requirements, Feature Stability, and Resolution," Annual Review of Materials Research, Vol 40 40, 395-414 (2010).
18. J. Brünahl, and A. M. Grishin, "Piezoelectric shear mode drop-on-demand inkjet actuator," Sensors and Actuators A: Physical 101, 371-382 (2002).
19. ANP, "http://www.anapro.com/kor/product/Products_Information_Advanced_Nano_Products_v1.pdf

?PHPSESSID=19c9b659988a71075589ee2faa9093a2." published by ANP Co. Ltd., S. Korea (2012), Access date: 2012-11-20
20. Inktec, "http://www.inktec.com/english/pdf/upload_pdf/(E)Electronic_Ink_3.3_72dpi(2).pdf." published by InkTec Co. Ltd., S. Korea (2012), Access date: 2012-11-20
21. M. Mark Allen and Jaakko Leppäniemi and Marja Vilkman and Ari Alastalo and Tomi, "Substrate-facilitated nanoparticle sintering and component interconnection procedure," Nanotechnology 21, 475204 (2010).
22. M. Hummelgård, R. Zhang, H. E. Nilsson, and H. Olin, "Electrical sintering of silver nanoparticle ink studied by in-situ TEM probing," PLoS One 6, e17209 (2011).
23. M. L. Allen, M. Aronniemi, T. Mattila, A. Alastalo, K. Ojanperä, M. Suhonen, and H. Seppä, "Electrical sintering of nanoparticle structures," Nanotechnology 19, 175201 (2008).
24. A. Moliton, and R. C. Hiorns, "Review of electronic and optical properties of semiconducting π-conjugated polymers: applications in optoelectronics," Polymer International 53, 1397-1412 (2004).
25. J. Enevold, "Development of light-emitting electrochemical cells for novel applications," in Dept. of Physics(Umea University, 2012).
26. L. Basiricò, P. Cosseddu, B. Fraboni, and A. Bonfiglio, "Inkjet printing of transparent, flexible, organic transistors," Thin Solid Films 520, 1291-1294 (2011).
27. M. Neophytou, W. Cambarau, F. Hermerschmidt, C. Waldauf, C. Christodoulou, R. Pacios, and S. A. Choulis, "Inkjet-printed polymer–fullerene blends for organic electronic applications," Microelectronic Engineering 95, 102-106 (2012).